11

Mechanical Behavior and Plastic Instabilities of Compressed Al Metals and Alloys Investigated with Intensive Strain and Acoustic Emission Methods

Andrzej Pawełek
Aleksander Krupkowski Institute of Metallurgy and Materials Science
Polish Academy of Sciences, Kraków,
Poland

1. Introduction

The aim of the present chapter has been to substantiate and explain the relation among the behavior of acoustic emission (AE) parameters, the course of external load, evolution of microstructure and the dislocation mechanisms of slip and the localization of deformation connected with twinning, formation of slip and shear bands. The problem is of fundamental meaning, when qualitative and quantitative relations between the rate of AE events, amplitude and energy of AE signals and other AE descriptors in relation to micro-processes occurring in a material are to be discussed.

It is commonly believed that twinning is the most efficient source of acoustic emission (Bidlingmaier et al., 1999; Boiko, 1973; El-Danaf et al., 1999; Heiple & Carpenter, 1987; Tanaka & Horiuchi, 1975) due to fast release of great amount of elastic energy. It is connected with the fact that the velocity of twinning dislocations is higher than this of slip dislocations (Boiko, 1973), which results in the increase of contribution of accelerating effects in the recorded AE impulses.

One of the first AE investigations concerned the tensile test of titanium and its alloys (Tanaka & Horiuchi, 1975), in which it was established, that the AE activity in Ti was bound with twinning from the beginning, while in Ti alloys the AE impulses from twinning appeared after a high degree of deformation. During compression of the γ-TiAl alloy, AE sources were identified as generally coming from slip, twinning and the propagation of microcracks. It was reported, however, that the detailed mechanisms by which moving dislocations create elastic waves are still not fully understood (Bidlingmaier et al., 1999).

Moreover, the problem of twinning in Al has still remained controversial. It is believed quite commonly, that at least in simple uniaxial strain state, like in a tensile test, twins do not appear in Al. One of the aim of this chapter is to demonstrate, that there are numerous proofs, that in a complex strain state, which occurs in the channel-die compression of single Al crystals at temperature of liquid nitrogen the twinning processes do occur.

The reasons for undertaking such a research are numerous. At first, there is lack in literature of the experimental data on the AE behavior during channel-die compression of single

crystals. Secondly, in the contemporary materials science, one of the basic problems of plastic deformation of metals are questions of strain localization due to the formation and development of slip lines and slip bands as well as shear banding and twinning processes.
In the last decade the methods of intensive strain have become more and more widely used to obtain microstructure refinement and finally ultra fine-grained (UFG), nanocrystalline materials which have the excellent mechanical properties, such as great strength and plasticity or even superplasticity occurring in the conditions of relatively not too high temperatures (Vinogradov, 1998). They allow obtaining massive samples of metals ready for a further treatment. This refers in particular to the packet rolling with bonding, so called ARB (Accumulative Roll-Bonding) method (Saito et al., 1999; Pawełek et al., 2007). There are also known products obtained on industrial scale by the method of channel compression ECAP (Equal Channel Angular Pressing), (Kuśnierz, 2001). The method of torsion under high pressure HPT (High Pressure Torsion), (Valiev et al., 2000) has been the least known since obtaining the high pressure itself is a difficult problem.
The subject concerns the Al alloys of AA6060, AA2014 and AA5182 type as well as AA5754 and AA5251 ones. The examinations of Al alloys of AA6060 and AA2014 types were carried out applying the HPT method as well as ECAP technique with circular cross section of the channel. The anisotropy of Portevin-Le Châtelier (PL) and AE effects was described and the relation between the PL and AE effects in UFG (nanocrystalline) Al alloy after intensive strain processing was reported here for the first time.
On the other hand the results of the examinations of Mg-Li and Mg-Li-Al alloys, presented here for comparison, were carried out applying HPT method (Kúdela et al., 2011) as well as ECAP technique (Kuśnierz et al., 2008) with squared cross section of the channel.
The aim of this chapter has been also an attempt to present the correlations between the mechanisms of plastic deformation and the AE phenomenon and the discussion of the connection of AE with the possible phenomenon of superplasticity in UFG (nanocrystalline) aluminium alloys.

2. Materials and methods

2.1 Production of single and bi-crystals

The Al crystals of several different crystallographic orientations were obtained using a standard Bridgman method, while the Al bi-crystals of crystallite orientations {100}<011>/{110}<001> (Goss/shear) were produced applying a modified Bridgman technique of horizontal crystallization.
The samples of Al single- and bi-crystals, of dimensions 10x10x10mm of various orientations were cut out and subjected to tests of channel-die compression at room and liquid nitrogen temperature (77K) using an INSTRON testing machine equipped with channel-die (Fig. 1), which ensured plastic flow merely in the normal direction (ND) and in the elongation direction (ED), parallel to the channel axis, since the deformation in the transverse direction (TD) was held back by the channel walls.
The samples were deformed in a multi-stage way in order to obtain appropriate values of intermediate and final degrees of deformation. After each deformation stage they were trimmed to satisfy the slenderness ratio. In each case the traverse speed of the testing machine was 0.05 mm/min.
An apparatus recording the AE descriptors was coupled with the testing machine. Both systems are unique, fully computerized set for a simultaneous measurement of external

compressive force and AE descriptors. A broad-band piezoelectric sensor recorded AE signals in the range from 100 kHz up to 1 MHz. The contact of the sensor with the sample was maintained with the aid of steel rail which served as a washer in the channel-die, as well as an acoustic wave-guide. In order to eliminate unwanted effects of friction against the wall of the channel, each sample was covered with a Teflon foil. The more detailed description of the AE method is presented in the next section 2.2.

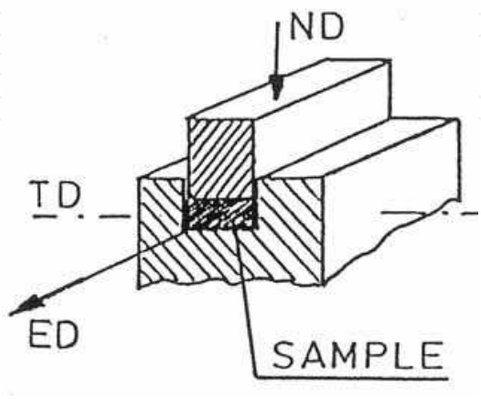

Fig. 1. Scheme of the device for the channel-die compression test

2.2 Acoustic emission method

The AE phenomenon takes place during a rapid release of elastic energy, accumulated in the material as a result of acting external or internal conversions, which can be emitted in the form of elastic waves which the frequency is contained between several kilohertz and a few megahertz. In metals and alloys, in general, they are generated as the effect of plastic deformation and particular dislocation strain mechanisms. The AE method enables sensitive monitoring effects in real time, even in considerable volume of investigated elements.

Considering simplifying assumptions, that the function of amplitude of strain field changes in the AE source has a form of elementary shock, the point of observation is in a distant area, and the elastic wave propagates in a homogeneous medium, the elementary equation of the signal propagation distance given in literature (Resnikoff & Wells, 1998) takes the form:

$$G(x,\ t'-t;x)=\frac{1}{4\pi\rho\, v_p^2}\,\gamma_i\,\gamma_j\,\frac{1}{r}\,\delta(t'-t-r/v_p) - \frac{1}{4\pi\rho\, v_s^2}\,(\gamma_i\,\gamma_j-\delta_{ij})\,\frac{1}{r}\,\delta(t'-t-r/v_s) \tag{1}$$

where: G_{ij} ($\boldsymbol{r}'$,t'-t;$\boldsymbol{r}$) is Green function for the displacement in directions x_i', y_i', z_i' in point $\boldsymbol{r}'$, in time t', in the case, when a local disturbance of strain field in point $\boldsymbol{r}$ in time t becomes the source of the displacement, ρ – medium density, v_p – velocity of dilatation wave, v_s – velocity of shear wave, γ_i, γ_j - for i=1, 2, 3 and j=1, 2, 3 are directional cosines source-receiver and receiver-source, r – distance between AE source and sensor, δ_{ij} – Kronecker delta, $\delta(x)$ – delta function equal $+\infty$, for x=0 and equal 0 for the remaining values x.

Apart from the AE signal the apparatus registers also a noise of acoustic background and that generated during the processing of the recorded signal. In the course of its processing from the analogue form into digital one, so called *quantization noise* occurs, resulting from

the process of rounding the instantaneous value of the signal to the levels, which are the components of a binary form of the record. The decrease of quantization noise was attained through the use of modern analogue-numerical processors of high linearity of processing and resolution of 12 bytes in an optimal range of input voltages of about ±5V.

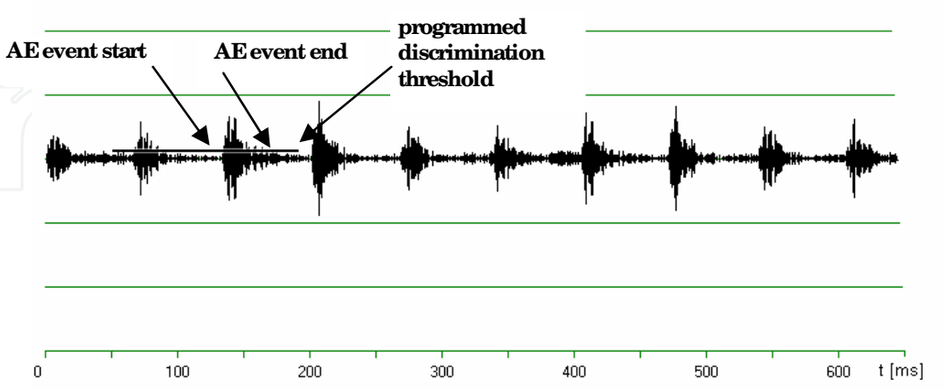

Fig. 2. The principles of AE event detection

The line determining the maximum level of noise voltage of surrounding background is shown in Fig. 2. The level is taken as a discrimination voltage. The occurrence of AE is defined as a moment of increase of instantaneous signal value above the discrimination voltage. The duration of the AE event is determined to the moment of the decrease of instantaneous signal value below the discrimination voltage. The method takes into account the detection of events with the possibility of software increase/decrease of the discrimination level voltage (Paupolis, 1980). The applied algorithm of AE event detection enables a program implementation of numerical records of signals containing even a few hundred of megabites. By means of such an algorithm, it is possible to detect the events lasting at least three times the sampling period of the applied analogue-numerical processor. For example, for the frequency of sampling used at present in long-lasting examinations, which is 88.2kHz, the minimum duration time of an event is 34 microseconds. A 9812 ADLINK fast card of analogue-numerical processor was used for the analysis of AE signals. Such a device enables the increase of instrument sensitivity and detection of AE events differing by an order of magnitude. The indexes of start and end of AE event recorded in the program table can serve to the determination of its duration. The E energy of AE event can be derived from the approximate formula:

$$E = 0.5\ (\nu_{max})^2\ \Delta t, \tag{2}$$

where ν_{max} denotes maximum value of AE signal during the event, Δt – time of AE event.
To characterize the material subjected to the examinations, values of arithmetic means of all measured values E, ν_{max} and Δt are needed. The AE instrument is also equipped with an analogue system, which allows obtaining an effective value of the signal.
The transformation of the set of instantaneous values of the measured $v(t)$ signal into effective value V_{RMS} for time T is realized according to formula:

$$V_{RMS} = \sqrt{\frac{1}{T}\int_0^T \nu^2(t)dt}. \tag{3}$$

The AE signals generated by different sources in the examined object can be analyzed inspecting the changes of its *spectral characteristic*. A continuous AE signal $v(t)$ in a selected finite range of time can be demonstrated as a function of its spectral characteristic $A(\omega)$, where ω is a frequency pulsation f, defined as $\omega=2\pi f$. Assuming absolute integrality, function $v(t)$ is linearly transformed into the function of spectral density $A(\omega)$ according to the Fourier transformation:

$$v(t) = \frac{1}{\pi}\int_0^{\infty} A(\omega)\exp(j\omega)d\omega. \tag{4}$$

In consequence, the procedure of spectral density function determination $A(\omega)$ for consecutive segments of discrete set of AE signal samples was elaborated together with a corresponding graphic presentation of results in the form of acoustic maps i.e. *acoustograms* or *spectrograms*. A numerical method of Windowed Fourier Transformation (WFT) is applied here. Next, the discrete form of spectral density function is determined using several thousands of signal samples adjacent to the central sample of the recorded AE event. The algorithm, which transforms the set of signal samples into a set of spectral density coefficients $c_n : v(m) \Rightarrow c_n(\omega)$ is similar to the approximate formula (Scott, 1991):

$$c_n \approx \frac{1}{N}\sum_{m=0}^{N-1} v(m)\cdot \mathrm{mod}(e^{jn2\pi m/N}), \tag{5}$$

in which j denotes $\sqrt{-1}$ and mod is the module of complex expression.
The acoustogram of AE event set presented earlier in dependence of signal amplitude on time in Fig. 2 has now been shown in Fig. 3. The spectral characteristic of signal is illustrated every 0.5ms. The discrete equivalent of the $A(\omega)$, spectral density function is presented in the form of color code.
The AE analyzer is equipped with an additional measurement channel enabling simultaneous recording of sample load by the computer as well as the registration of AE parameters in the form of AE event rate together with their duration, amplitude and effective value connected with conventional value of the event energy and in consequence, the distribution of events number versus their energy.

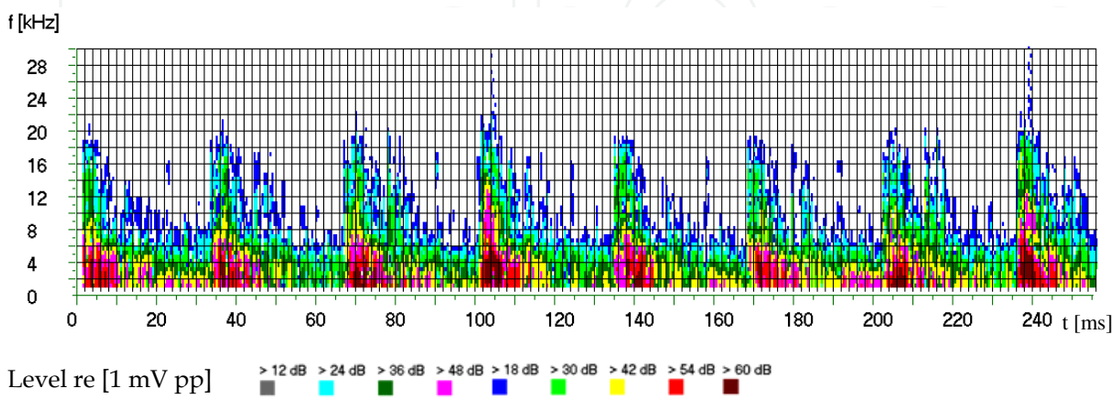

Fig. 3. Acoustogram of AE event set, previously presented in Fig. 2 in the form of dependence of signal amplitude on time

The effective value of noises at the inlet of the preamplifier is about 20÷30mV, depending on the selected frequency band. During the signal processing the value undergoes about four-fold decrease due to the application of a band-pass filtration. An active upper-pass filter of 8th order of cut off frequency 5kHz is joined to the preamplifier. Another filter of 4th order of 20kHz frequency can be additionally switched on. Thanks to that, the signals of a vibroacoustic background, which do not originate from the processes occurring because of sample loading, are eliminated from the further processing. The signal is next passed to a lower-pass filter of cut-off frequency 1MHz. The total amplification of AE signal at the outlet of instrument is 70dB and the threshold voltage is 0.5V. The effective voltage value of the AE signal recorded is derived through the second exit. The analysis of energy and duration of individual AE events is possible with an appropriate program, which determines time of the AE event occurrence, its maximum amplitude, sum of recorded amplitudes and duration time of the event up to significant decrease of its amplitude.

2.3 Methods of microstructure observations

After each stage of a compressive test, microstructure observations were carried out using a standard technique of optical microscopy at NEOPHOT instrument. The further observations were performed using transmission (TEM) and scanning (SEM) electron microscopes. The techniques of *convergent beam electron diffraction* (CBED) and *electron back scattered diffraction* (EBSD) as well as SEM with *field emission gun* (FEG) were applied in the examinations of bi-crystals.

2.4 Methods of intensive deformation

Fig. 4a shows the scheme of the ECAP method. The parameters of the installation have the following values: b=10mm, a=30mm, angle α=31.3° or α=90°. Equivalent strain (for square cross-section) is equal to ε_n=0.5922n, where n – number of passes. For angle Φ= 90° and α=0 it amounts to ε_n=0.9069n.

Fig. 4b shows the scheme of the HPT method of torsion under high pressure. The sample is in the form of a roll with R radius and the height l. Dilatation strain γ after N rotations is equal to $\gamma=(2\pi RN)/l$, and the equivalent strain $\varepsilon_N=\gamma/1.73$.

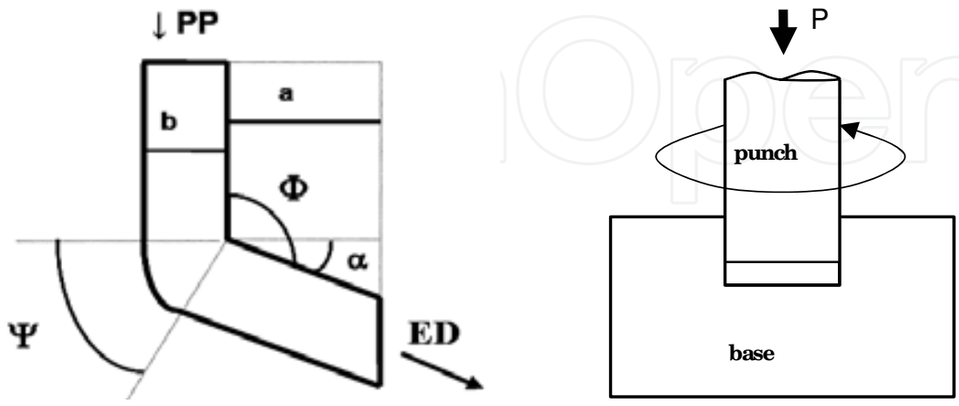

(a) (b)

Fig. 4. Scheme of ECAP (a) angular extrusion: ED – direction of outflow, PP – direction of punch pressure and the scheme of the HPT process (b)

Fig. 5 presents the scheme of the ARB technique. Purified and degreased surfaces of two sheet plates are folded and fastened, next heated and rolled to reduction z = 50%. The sheet obtained after rolling is cut into halves and subjected to the same procedure as before. The procedure may be repeated several times. For example, a sheet plate with thickness g_o, subjected to rolling in succession n time to the reduction of z=50%, i.e. after n passes, has thickness $g_n=g_o/2^n$, and the total reduction is equal to $z_n=1- g_n/g_o=1-1/2^n$. The tensile tests were carried out with ten-fold plane specimens using the standard INSTRON machine. The rate of the traverse of the testing machine was 2mm/min. Each specimen was of gauge length l_0=90mm (overall length l_c=105mm), b_0=20mm wide and a_0=3.50mm thick.
The samples for ECAP tests (for circular cross-section) had the shape of rolls with diameter 20mm and height 30÷40mm while that for the ECAP processing in the channel of square cross section was in the shape of rectangular prisms of dimensions 10x10x40mm. The samples to be used in HPT tests had the shape of discs of diameter 10mm and thickness 3÷5mm. The samples intended for compression had the shape of cubes with the edge not greater than 10mm in the case of ECAP or the shape of square plates with side 10mm and thickness 1mm, cut in the case of ARB from the samples prepared earlier for the tensile tests. The discs after HPT, intended for the compression, had the thickness of the order of 1÷2mm.

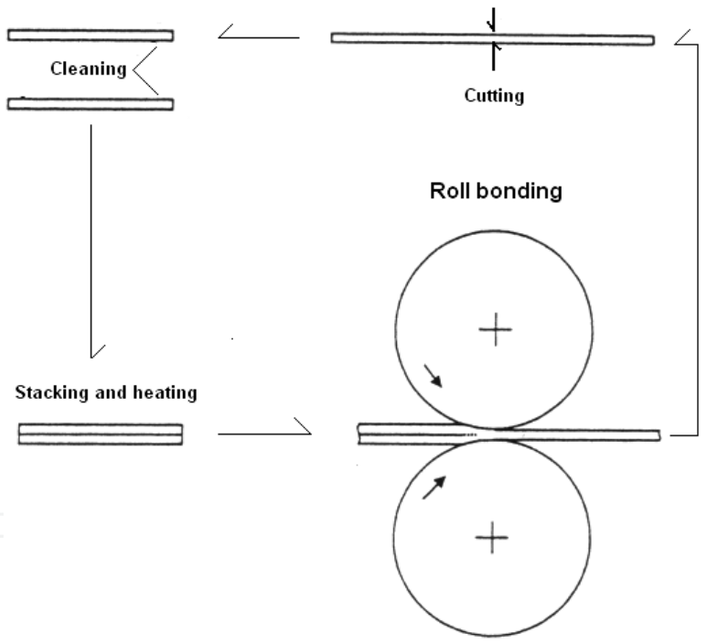

Fig. 5. Scheme of the ARB process

Simultaneously with the registration of the external force F and the sample elongation, the basic AE parameters in the form of AE event rates, or as RMS – the effective value of voltage of the registered AE signal were measured.
The aim of the research has been the documentation and interpretation of correlation of the AE descriptors during compression tests of Al alloys before and after pre-deformation by intensive strain methods. The evolution of micro- and/or nanostructure in dependence on dislocation mechanisms of deformation as well as slip processes occurring along grain boundaries, responsible for possible superplastic flow, is also considered.

3. AE in Al mono- and bi-crystals compressed at liquid nitrogen temperature

3.1 Twinning and shear band formation in Al single crystals

The examinations of AE in Al mono- and bi-crystals were aimed at the identification of unstable plastic flow mechanisms connected with the deformation twinning and the formation of shear bands. The compression test were carried out mainly at temperature of liquid nitrogen (77K). Moreover, the still controversial problem of deformation twinning in Al crystals is also considered here.

The course of AE and the external force in the Al crystal of Goss orientation {110}<001> is shown in Fig. 6a whereas Fig. 7 comprises, for the purpose of comparison, the results of AE and the course of external force for the crystal of {112}<111> orientation.

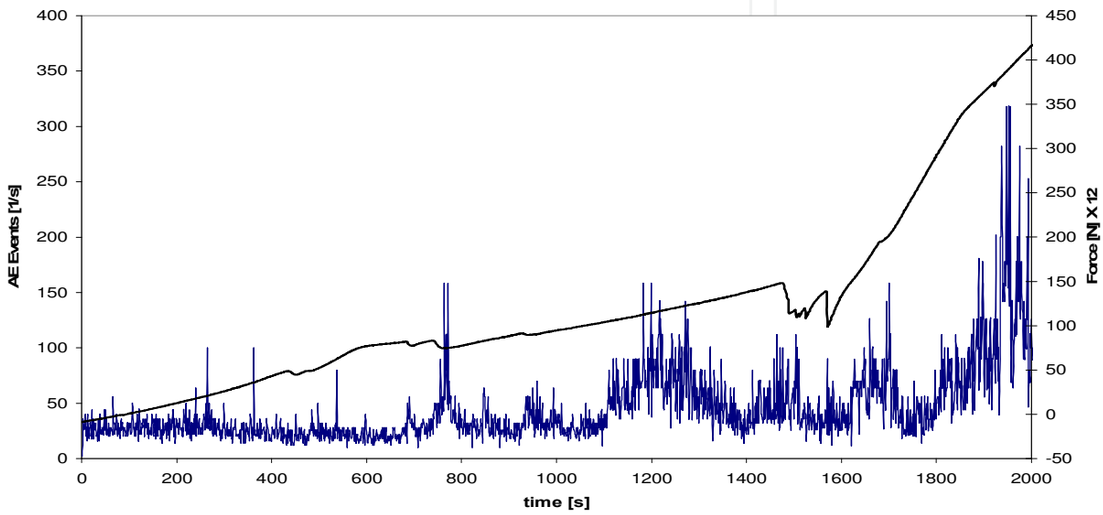

(a)

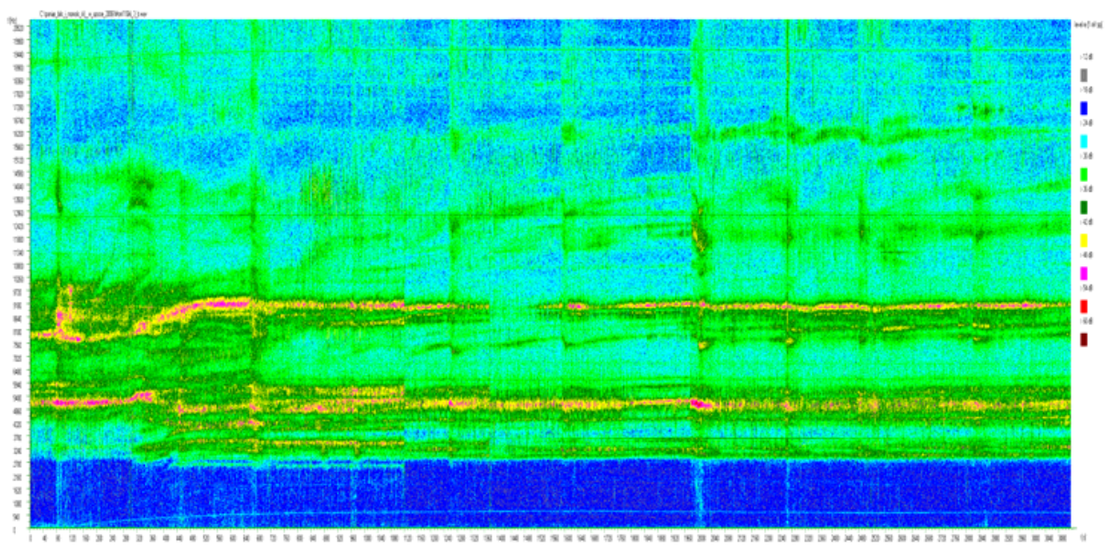

(b)

Fig. 6. Course of AE and compressive force in Al single crystal of Goss orientation (a) together with corresponding acoustogram (b)

When analyzing Fig. 6, it can be stated, that evident correlation exists between the course of force and behavior of AE. All the local decreases of the force curve are accompanied by more or less distinct areas of elevated AE activity. It seems that these strong plastic instabilities on the compression curve correspond to the occurrence of shear bands. Vertical areas in the acoustogram containing a broad range of frequency spectrum visible in Fig. 6b.
On the other hand, low temperature courses of AE impulses together with external compressive force in dependence on time are presented in Figs. 8 and 9a and 10a for the Al single crystals of two selected orientations: {112}<111> (Fig. 8) and {531}<231> (Fig. 9a for reduction z≅27.1% and Fig. 10a for reduction z≅51.4%). Attention should be drawn to some characteristic features of the recorded courses.
Moreover, the experimental {111} pole figures (EXP) presented in Figs.9b and 10b, as well as the calculated orientation distribution functions (ODF) referred to in Figs.9c and 10c, illustrate explicitly the existence of twin orientation after compression to z≅51.4% (Fig. 10b and 10c), and suggest strongly the possibility of deformation twinning also in the Al single crystals channel-die compressed at the liquid nitrogen temperature. In {111} pole figure (Fig. 10c), the component of twin orientation $(\bar{4}\,4\,1)\,[\bar{1}\,\bar{3}\,8]$, appearing after reduction z≅51.4% (initial matrix orientation $(\bar{1}\,3\,5)[\,\bar{1}\,3\,\bar{2}\,]$, Figs. 9b and 9c) is now given by orientation $(\bar{2}\,2\,5)[\,\bar{3}\,7\,\bar{4}\,]$ (Fig. 10c) – corresponds to the twinning on the active co-planar slip system.

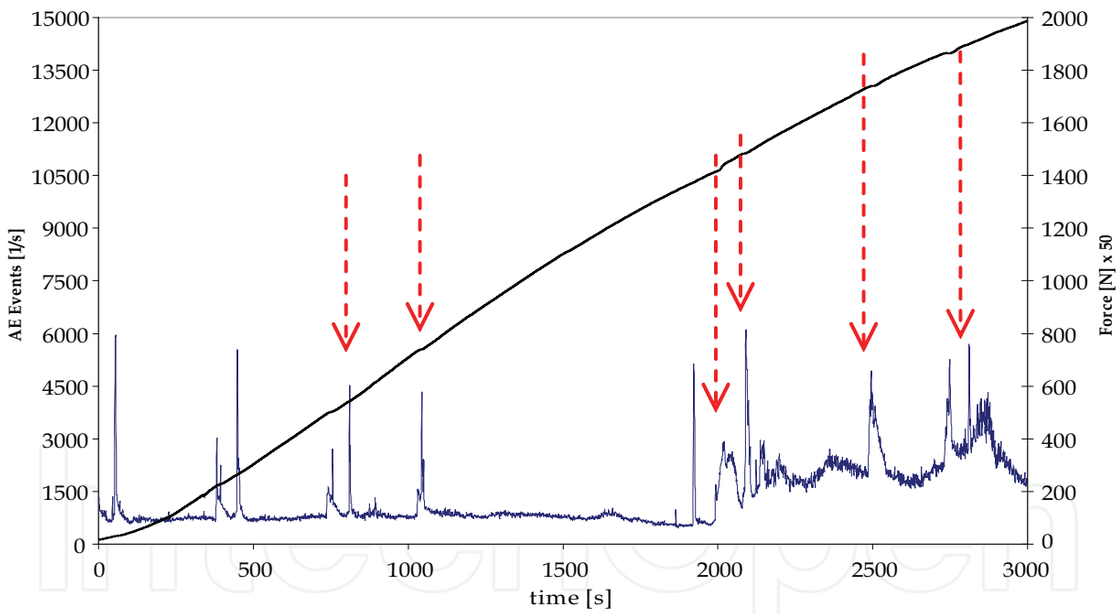

Fig. 7. Acoustic emission and compressive force in Al single crystal of orientation type C≡{112}<111>. The arrows indicate the correlations between AE and drops of force

Based on the dislocation dynamics and the AE model (Jasieński et al., 2010; Pawełek, 1988a; Pawełek et al., 2001; Ranachowski et al., 2006) a number of AE impulses, which were generated due to the appearance of an individual twin lamella can be estimated. It was assumed, that the twins formed as a result of the pole mechanism action. It was also accepted, that an individual AE impulse occurred, when a partial twinning dislocation, which moved in the area of a single atomic plane, approached the surface. This suggestion is in agreement with the results and concepts reported by Boiko et al. (1973, 1974, 1975) for the

relationship between AE and elastic twins generated in calcite crystals. It was also assumed for simplification that distance a between the atomic planes was equal to the value of Burgers vector of dislocation i.e. $a \cong b \cong 1.0 \times 10^{-4}$μm.

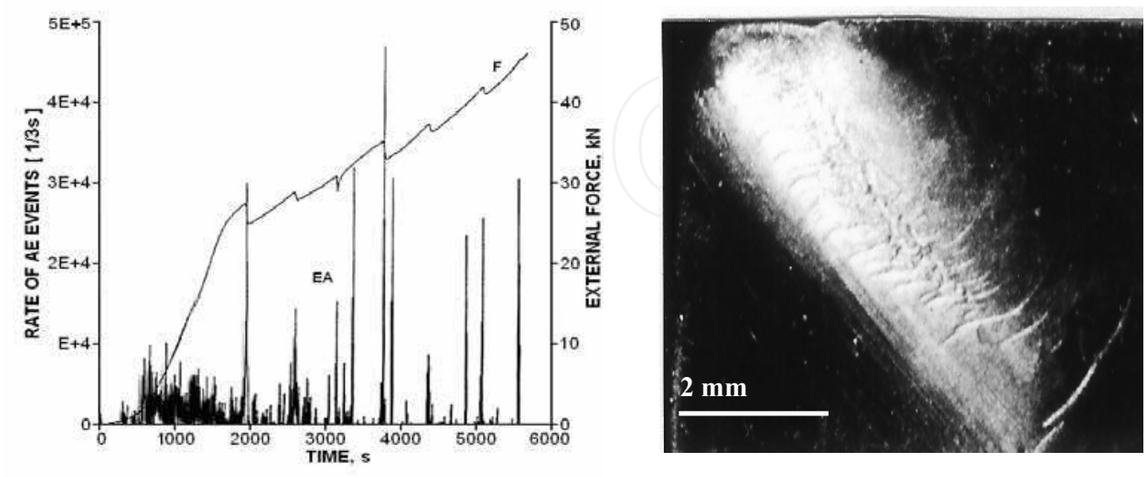

Fig. 8. Courses of AE and external force of Al single crystal of orientation {112}<111> channel-die compressed at T=77 K up to reduction z=61.6%; microstructure inserted nearby illustrates shear band

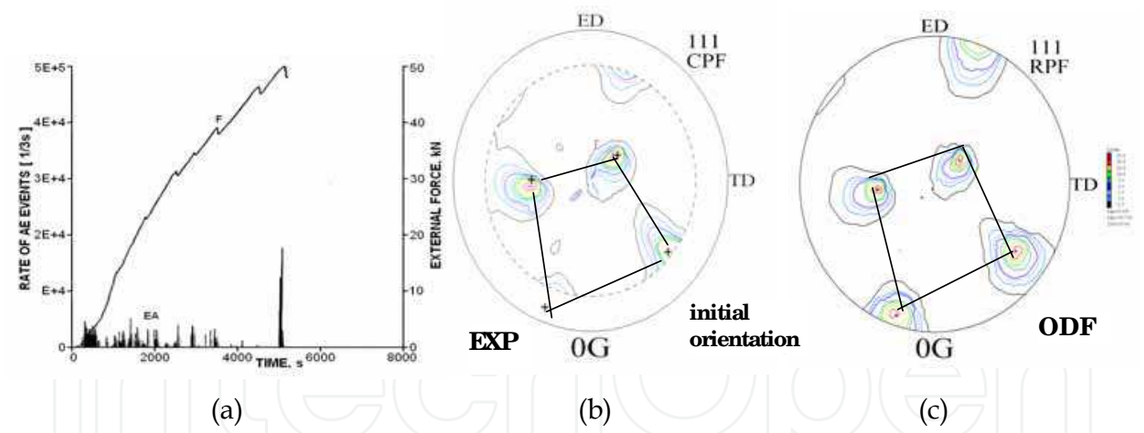

Fig. 9. Courses of AE and external force (a) of Al single crystal of initial orientation {531}<231> channel-die compressed at T=77K up to reduction z=27.1% and corresponding {111} pole figures: experimental EXP (b) and recalculated ODF (c)

The thickness of twin lamella, estimated visually from microstructure images, was in the range from 0.1μm up to 1.0×10^{3}μm, which, at magnifications of order 10x÷100x, used the most frequently, gave the thickness of a real twin lamella, at first approximation, in the range from 1 up to 100μm. Hence the number of atomic planes engaged and the number of elementary impulses completing the AE peak from an individual twin was of order $10^{4} \div 10^{6}$, which was in satisfactory agreement, as far as the order of value was concerned, with the value observed.

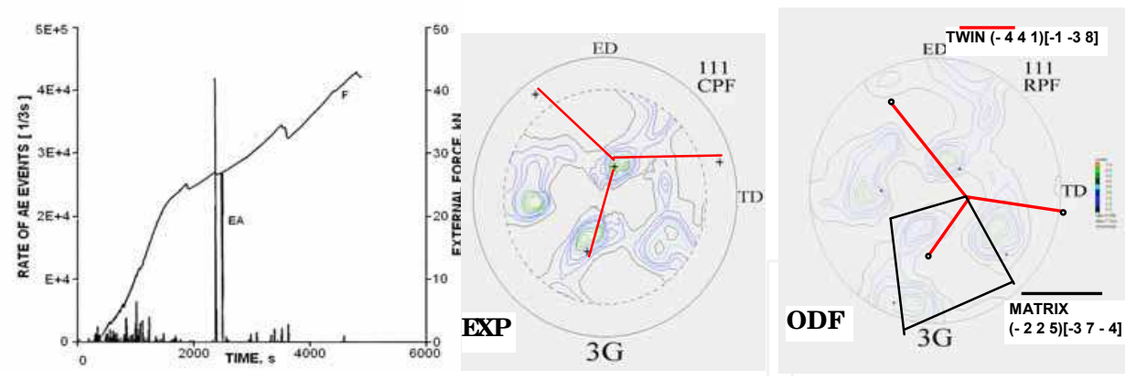

Fig. 10. Courses of AE and external force (a) of Al single crystal of initial orientation {531}<231> channel die-compressed at T=77K up to reduction z=51.4% and corresponding {111} pole figure experimental EXP (b) and recalculated ODF (c)

3.2 AE during channel-die compression of Al bi-crystals

The examinations of AE tests in Al bi-crystals subjected to low-temperature channel-die compression were also performed. Fig. 11 show the behavior of AE and force together with corresponding acoustogram for the Al bi-crystals of {110}<100>/{110}<011 hard/Goss orientation. After the first stage of deformation (z≅30%), the sample was trimmed and compressed again until it was reduced by z≅50%. Courses of AE and external force for a bi-crystal of {110}<001>/{100}<011> Goss/shear orientation are illustrated in Fig. 12 for the first stage of deformation (z≅20%). For such an orientation also structural examinations were performed using TEM and CBED and SEM-FEG/EBSD techniques.

3.3 Development of Al bi-crystal dislocation structure

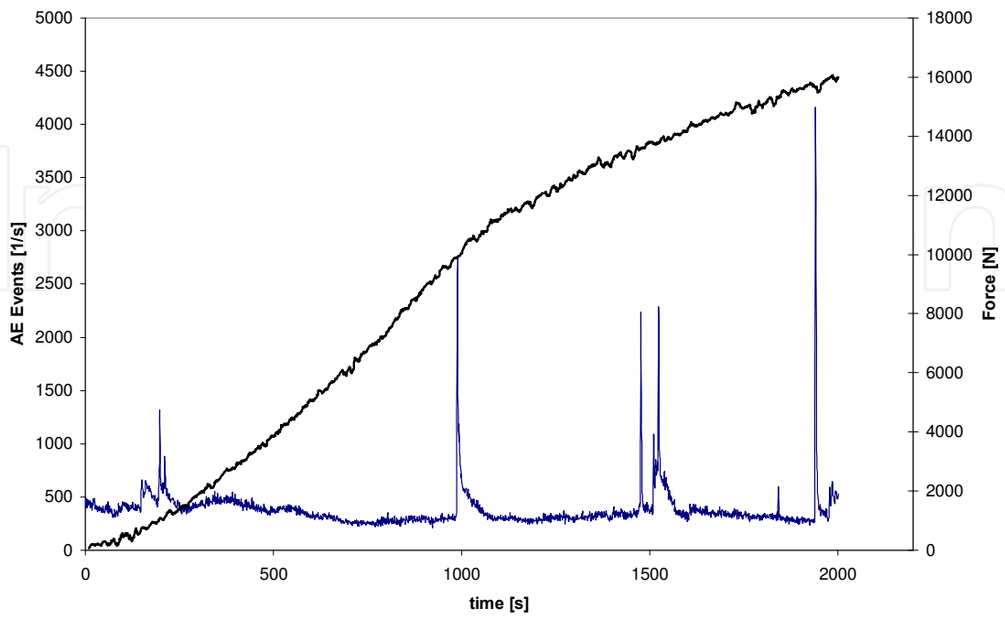

(a)

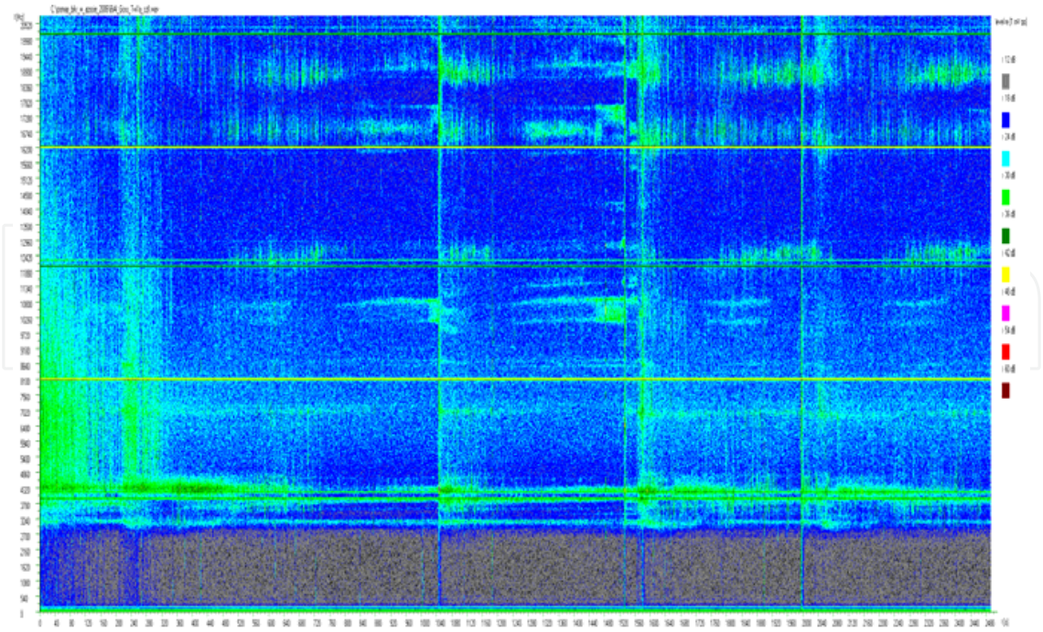

(b)

Fig. 11. AE and force of channel-die compressed Al bi-crystal of {110}<100>/{110}<011> hard/Goss orientation reduced by z≅50%: (a) and corresponding acoustogram (b)

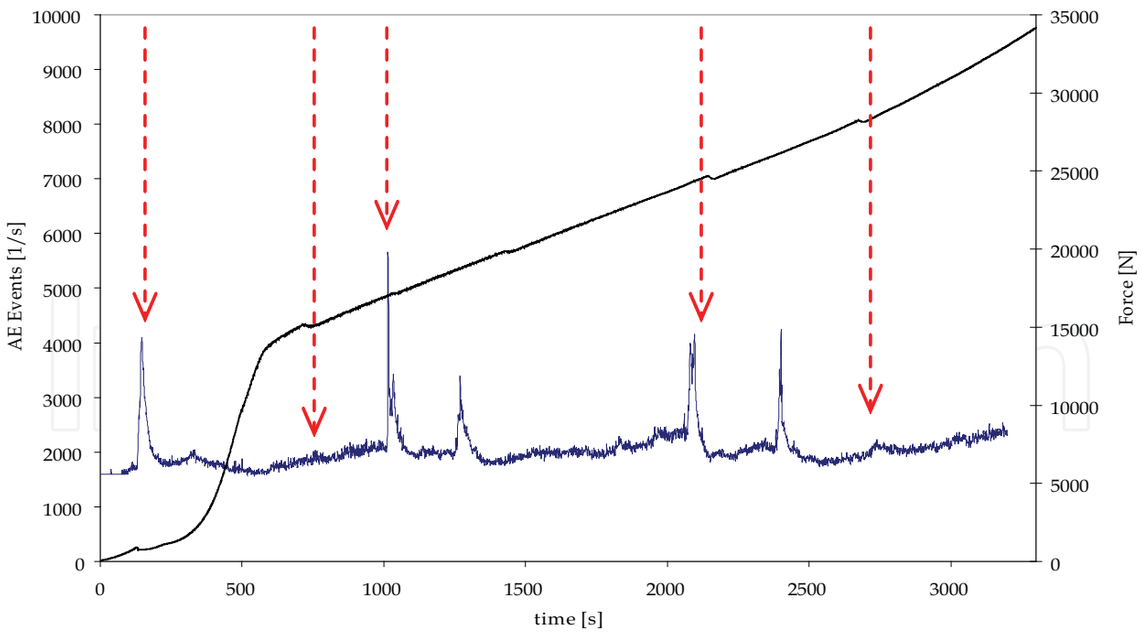

Fig. 12. Behavior of AE and compressive force of bi-crystal of {110}<001>/{100}<011> Goss/shear orientation. The arrows indicate the correlations between AE and drops of force

The Goss {110}<001> orientation remained stable during compression in a broad range of deformations, while the shear {100}<011> orientation was strongly unstable and underwent

decomposition from the initial stages of deformation by rotation around the transverse direction (TD).

3.3.1 TEM microstructure observations

The examinations in the micro and mezzo- scale were focused on the structure and texture analyses carried out using transmission (TEM) and scanning (SEM) electron microscopy. In both cases, the observations were correlated with measurements of local orientations changes with the use of *convergent beam electron diffraction* (CBED) and *electron back scattered diffraction* (EBSD) techniques. The TEM orientation measurements were performed using semi-automatic system, while the SEM instrument equipped with field emission gun (FEG) disposed of fully automated system Channe 5™ of HKL Technology firm.

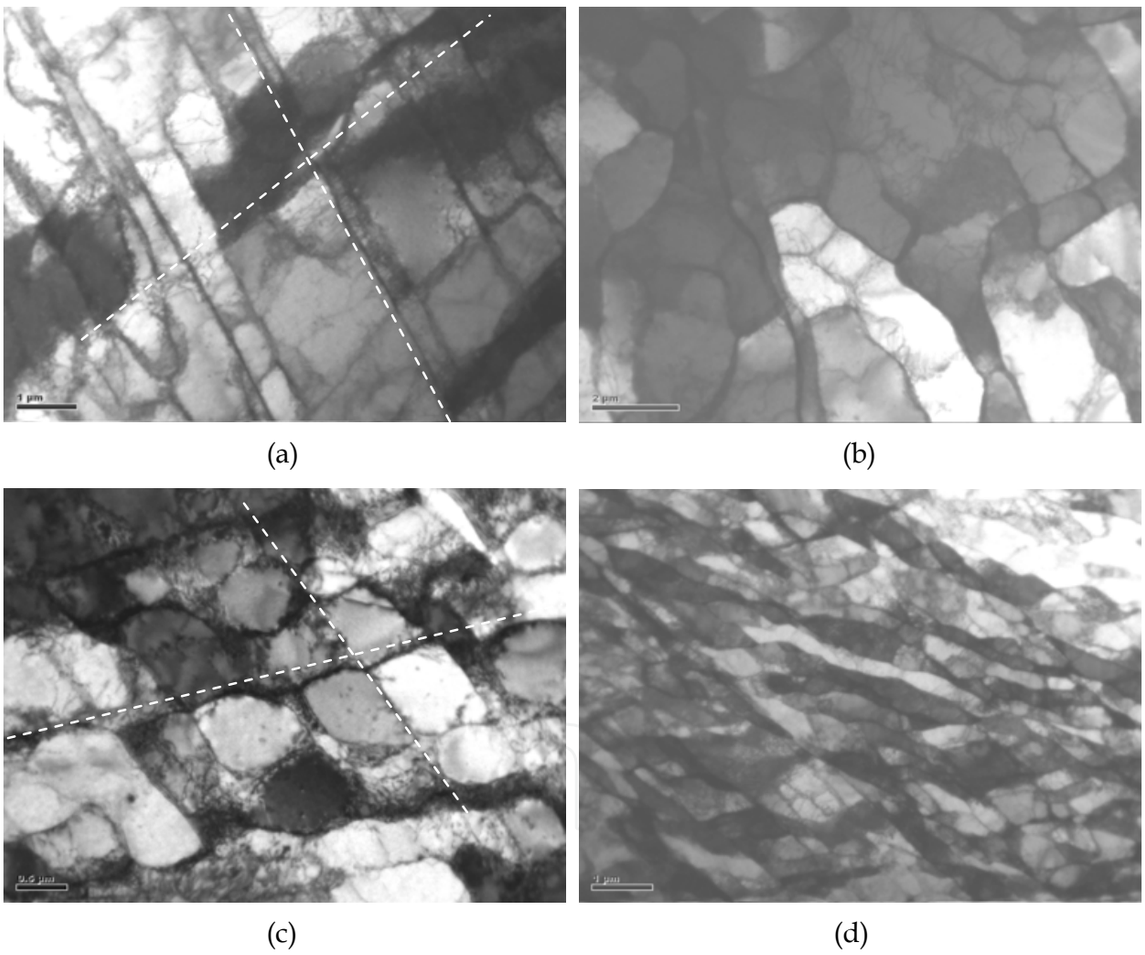

(a) (b)

(c) (d)

Fig. 13. Development of dislocation structure observed in TEM in crystallites of Al bi-crystal; (a) and (c) Goss orientation, (b) and (d) shear orientation; total deformation of bi-crystal z≅20%(c) and z≅70%(d). In the Goss orientation traces of planes, on which active slip systems operated are marked

The observations of dislocation structure in TEM in each crystallite of the bi-crystal deformed by z≅20% and z≅70% were correlated with the local orientation measurements in

a high-resolution scanning microscope using SEM-FEG/EBSD techniques. The development of dislocation structure observed in TEM is presented in Fig. 13 for each crystallite and for two deformation degrees. The advance of structure refinement together with the increase of deformation was observed in the crystallites with the Goss orientation {100}<011>. In crystallites of shear orientation {100}<011>, two pairs of coplanar slip systems were active what led to the decomposition of the crystal resulting in the change of initial crystallite orientation to two symmetrically situated positions of {112}<111> orientations. The areas, in which different slip systems dominated were separated by intermediate bands.

3.3.2 SEM examinations of local texture changes

The texture-structure examinations were performed using the SEM-FEG/EBSD system at a mezzo-scale, which allows reproducing the "electron" image of structure as regards the crystallographic orientation changes.

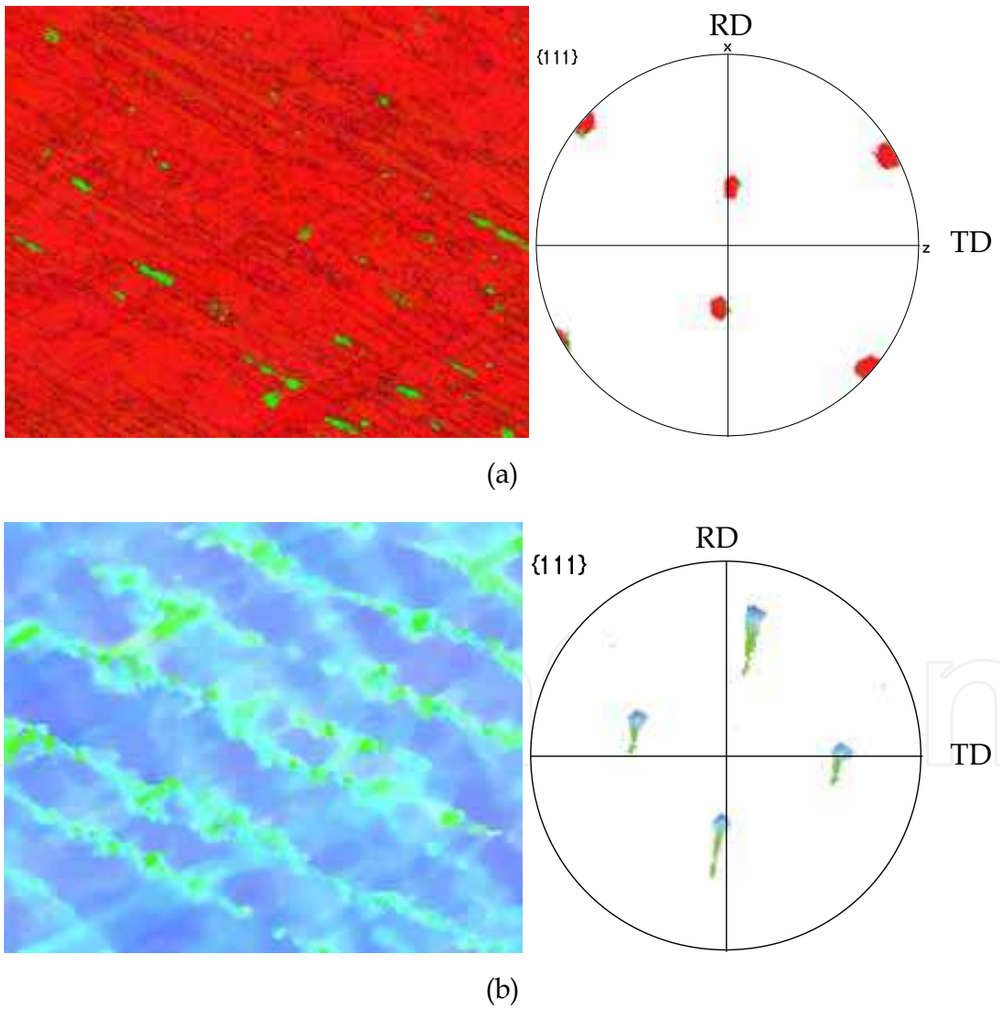

Fig. 14. Orientation maps (shown as a „function" of IPF colors) for the part of bi-crystal of Goss (a) and shear (b) orientation and corresponding {111} pole figure. Measurement step 100nm. Reduction z≅20%

The obtained orientation maps of Goss and shear type presented in Fig. 14 illustrate well the observed tendencies to broadening of the initial orientation of the crystallites in the bi-crystal. In the Goss orientation (Fig. 14a), after an applied deformation degree, initial orientation remains stable; only weakly visible tendency to broadening of the {111} plane poles mainly by a rotation around ND is observed. In the case of crystallite of orientation shear (Fig. 14b) a strong tendency to rotation of crystalline lattice through the rotation around TD, towards two complementary positions of the {112}<111> orientation. The presented orientation map shows the structure-texture changes in the area, in which one pair of coplanar systems dominates.

3.4 Comparison with other fcc single crystals

In order to document better the correlation between the AE behavior and the localization of deformation connected with twinning processes and the formation of shear bands, experiments at temperature of liquid nitrogen (77 K) were carried out on single crystals of Ag and Cu. The selected results for the Ag single crystals are presented in Fig. 15, and for copper in Fig. 16. The results refer to the same orientation {112}<111> and two subsequent

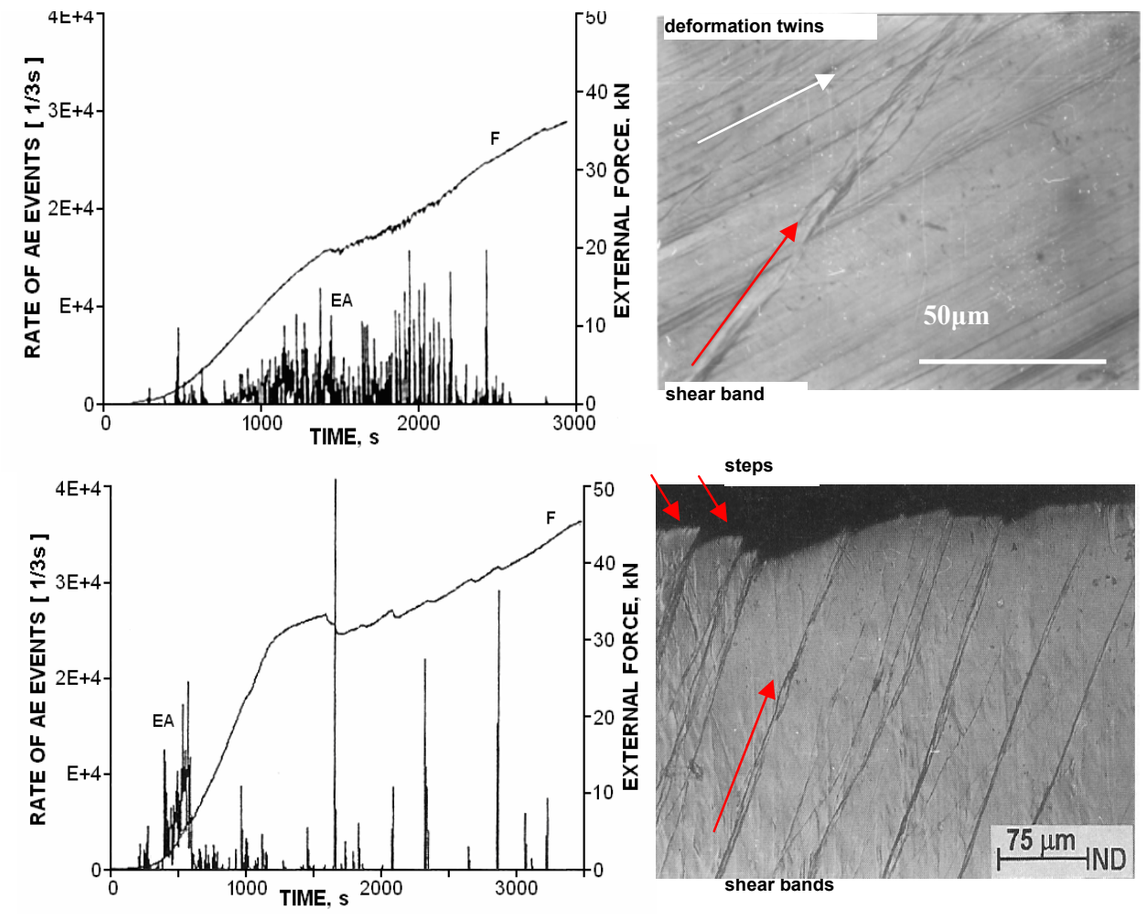

Fig. 15. Courses of AE and external force and corresponding microstructures of Ag single crystals of orientation {112}<111> channel-die compressed at T=77K: (a) – reduction z≅33% and (b) – reduction z≅63.4%

stages of compression, comprising conventionally intermediate reductions in the range from about 30% to 65%. It is visible, that the behavior of AE and its correlations with external loads are qualitatively very similar. It confirms that the deformation mechanism changes from an ordinary slip through strong twinning (Fig. 15a and 16a and appropriate optical microstructures) to the mechanism of shear band formation (Fig. 15b, 16b and corresponding optical images).

The considerable drop of AE event rate is a characteristic feature of twinning → shear bands transition, while corresponding high AE peaks are distinctly correlated with abrupt drops of the external load, which is the most evidently caused by the appearance and development of individual shear bands, which belong to the same primary family. For example, the last high AE peak visible in Fig. 16a at about 2200s may originate from an already forming shear band.

Comparing the courses of force and AE and the microstructure (Fig. 8) for the Al crystal of {112}<111> orientation with respective plots and images for the Ag and Cu single crystals of the same orientation (Fig. 15 and 16, respectively) and analyzing the courses of force and AE for the {531}<231> orientation in the Al single crystals (Figs.9a and 10a) a similarity to a large extent can be noticed, which lets us state, that also in the Al single crystals compressed at low temperatures, the transition of the type twinning → shear bands after initial slip deformation is quite probable.

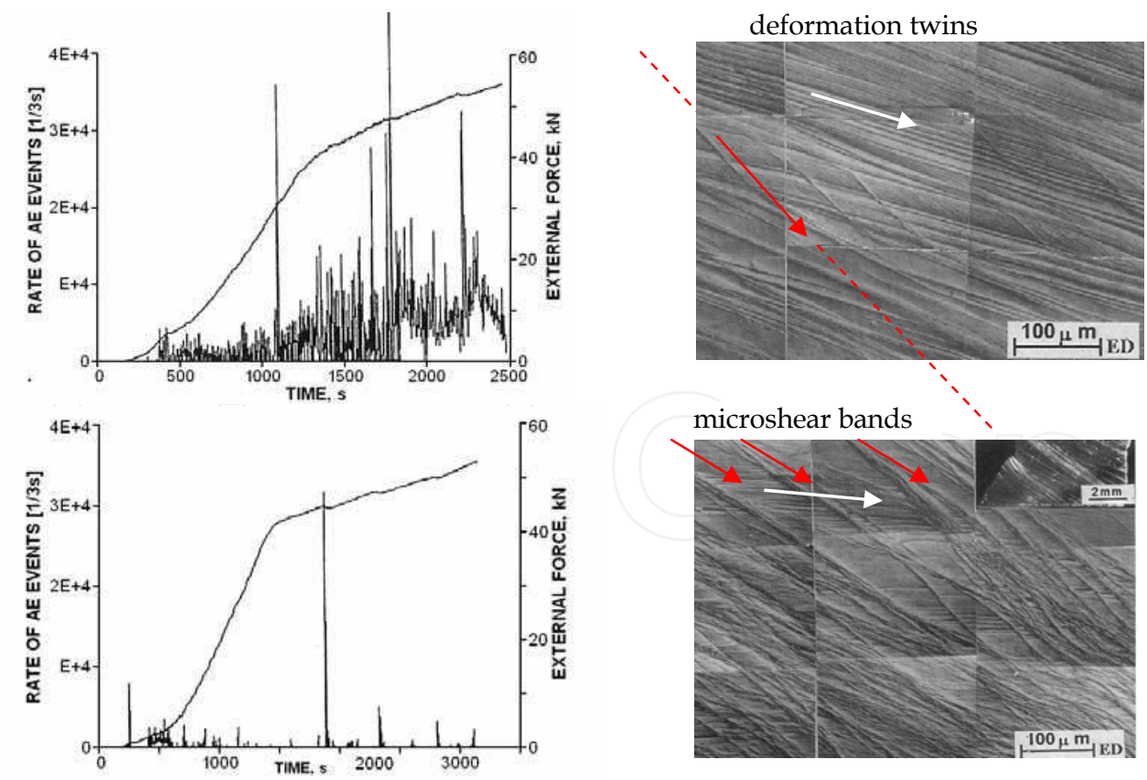

Fig. 16. Courses of AE and external force and corresponding microstructures of Cu single crystals of orientation {112}<111> channel-die compressed at T=77K: (a) – reduction z≅41% and (b) – reduction z≅53.4%

3.5 Acoustic emission vs. twinning in Al crystals

The presented results helped to establish a scheme of the microstructure evolution and mechanisms of deformation during channel-die compression of single crystals of fcc metals. The substantial element of the model is, that in the range of **intermediate reductions** (from about 30% to 65%) in the initial stages of compression, a change of the deformation mechanism from intensive twinning resulting in high AE of big activity of AE sources into the generation and localization of primary family of shear bands takes place. In the range of **small reductions** (up to about 35%) the dislocation mechanisms of ordinary slip dominate and processes of twinning can be initiated, while in the range of **high reductions** (above about 65%) the formation of another family of shear bands begins in the secondary slip systems, not coplanar with respect to the primary systems (Pawełek et al., 1997).

Based on the above considerations it can be stated, that the presented results directly indicated the correlation of the following four elements: high peak of AE event rate, abrupt decrease of external force, the formation of twin lamella or the nucleation of shear band as well as the appearance of a step at the surface of deformed crystal.

However, the twins were not observed neither in the Al crystals nor Al bi-crystals using the accessible methods of optical and electron microscopy. On the other hand the presented pole figures in Figs. 9 and 10 surely do not exclude the possibility of twinning. Moreover, they become a kind of proof that the process of deformation twinning in fact has occurred. It should be stressed that in this kind of discussion an argument is often raised, that the existence of twin orientations itself is not a proof that the process of deformation twinning has taken place. Similarly, the microstructures obtained using the TEM technique (Paul et al., 2001) may certify the fact that the deformation twinning occur also in single crystals of Al, although – it should be impartially said – they are not too convincing.

There is also another kind of confirmation of such a statement: it is the audible effect. In many cases, during the compression tests knocks typical for twinning were heard in the frequency range audible for the human ear. Hence, it is probable, that the difficulties in the documenting the twins in microstructure images are due to very high stacking fault energy of Al. Very fast processes of recovery or even recrystallization taking place in the sample being moved from the liquid nitrogen to the ambient temperature "blurr" the possible twins formed during deformation. In general the problem has not been definitely solved so far, although the results obtained may contribute, to some extent, to its full solution.

The observed correlations between AE and the mechanisms of deformation can be explained in terms of highly synchronized and collective behavior of groups of many dislocations, particularly in reference to the processes of dislocation annihilation at the free surface of the sample. Moreover, the description of dislocation annihilation based on the soliton properties of dislocation (Pawełek, 1988a; Pawełek et al., 2001) is closer to the reality than the description resulting from the application of the theory of continuous media (& Burkhanov, 1972; Natsik & Chishko, 1972, 1975).

4. AE in polycrystalline Al alloys deformed before and after intensive strain operations

4.1 AE in AA6060 and AA2014 alloys compressed before and after using the ECAP method

The measurement of AE were carried out for Al alloys of AA6060 and AA2014 type subjected to compression in a channel-die after the ECAP processing in a channel of circular cross-section. The AE behavior and the courses of compressive force of Al alloy of AA6060

type subjected to compression tests after 2- and 4-fold processing in the ECAP circular channel are presented in Figs. 17a and 17b, respectively, in which a significant decrease of AE level measured with the RMS parameter was observed. The observation confirms the

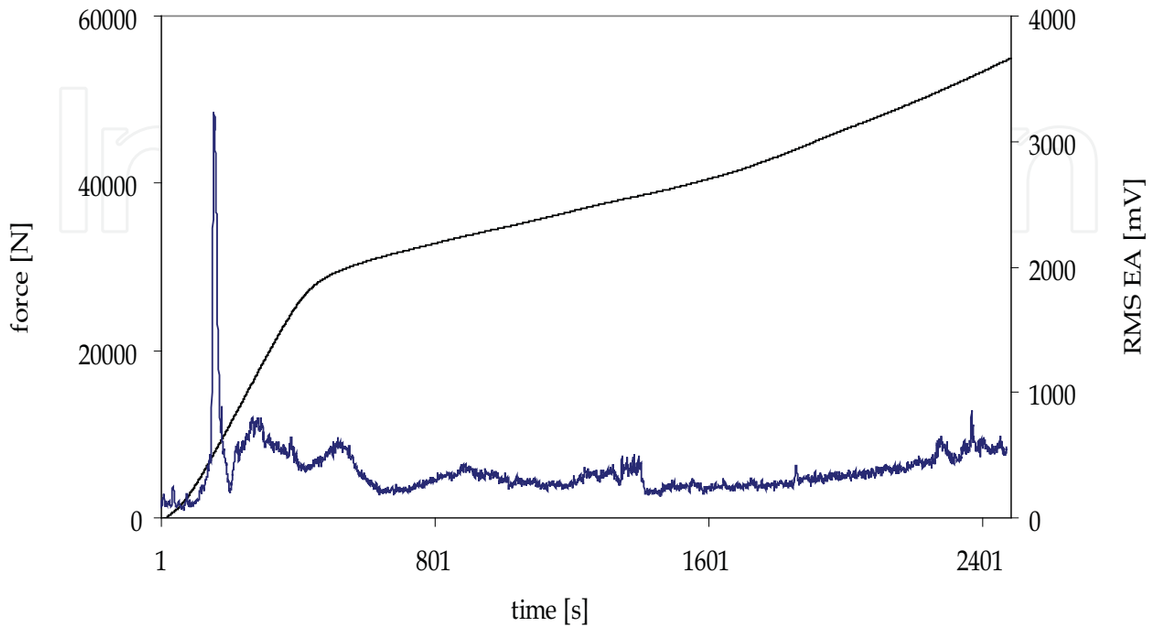

(a)

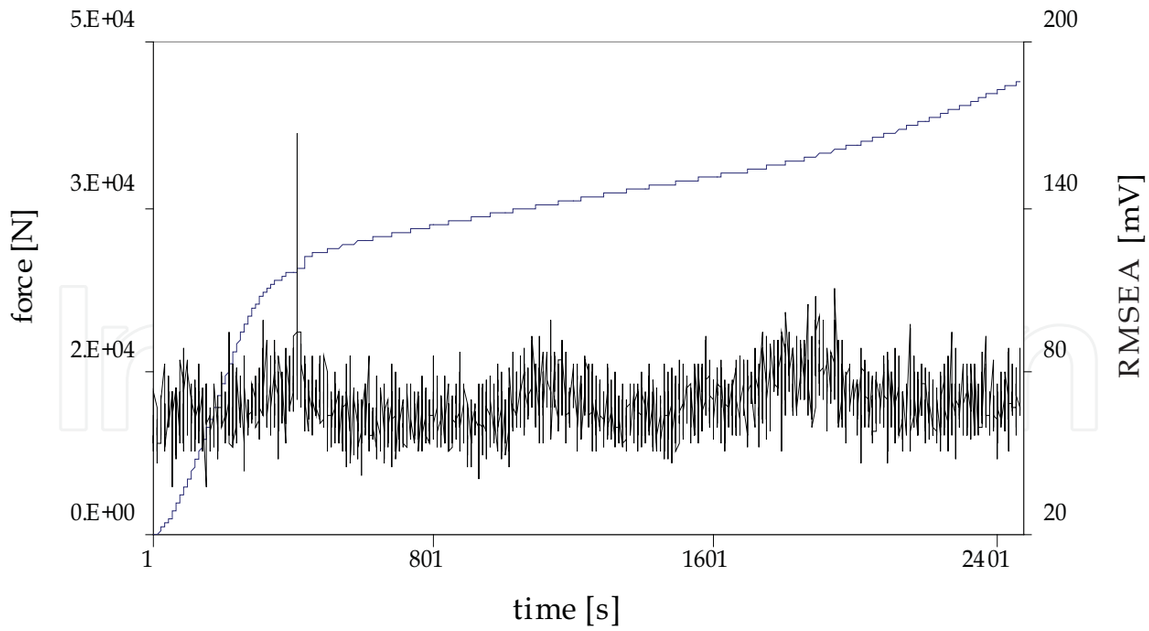

(b)

Fig. 17. AE and compressive force in Al alloy of AA6060 type subjected to tests of compression after two-fold (a) and four-fold (b) processing in the ECAP angular channel of circular cross section

tendency of AE to decrease reported earlier (Kúdela et al., 2011; Kuśnierz et al., 2008) in the samples of Mg-Li and Mg-Li-Al alloys compressed after processing with intensive deformation, and for comparison, presented here in the section 4.3 of this chapter. The next Figs. 18a and 18b show a TEM microstructure of the AA6060 alloy on horizontal and cross sections observed after 4-fold ECAP operation in the circular channel.
The results of AE examinations of the Al AA2014 alloy during compression tests are shown in Fig. 19 in which the courses of AE and external force in the sample after 2-fold processing in the angular circular channel ECAP (Fig. 19a) as well as the corresponding TEM microstructure (Fig. 19b) allow the conclusion, that the average level of AE is lower than in the AA6060 alloy, compressed also after 2-fold ECAP operation.

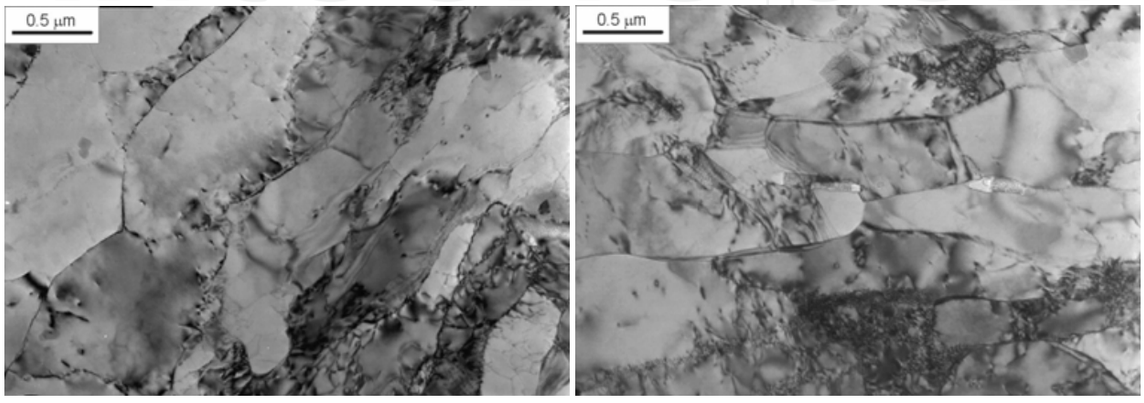

(a) (b)

Fig. 18. TEM microstructure of Al alloy of AA6060 type after 4-fold processing in the ECAP angular channel of circular cross section: (a) - horizontal section, (b) - cross section

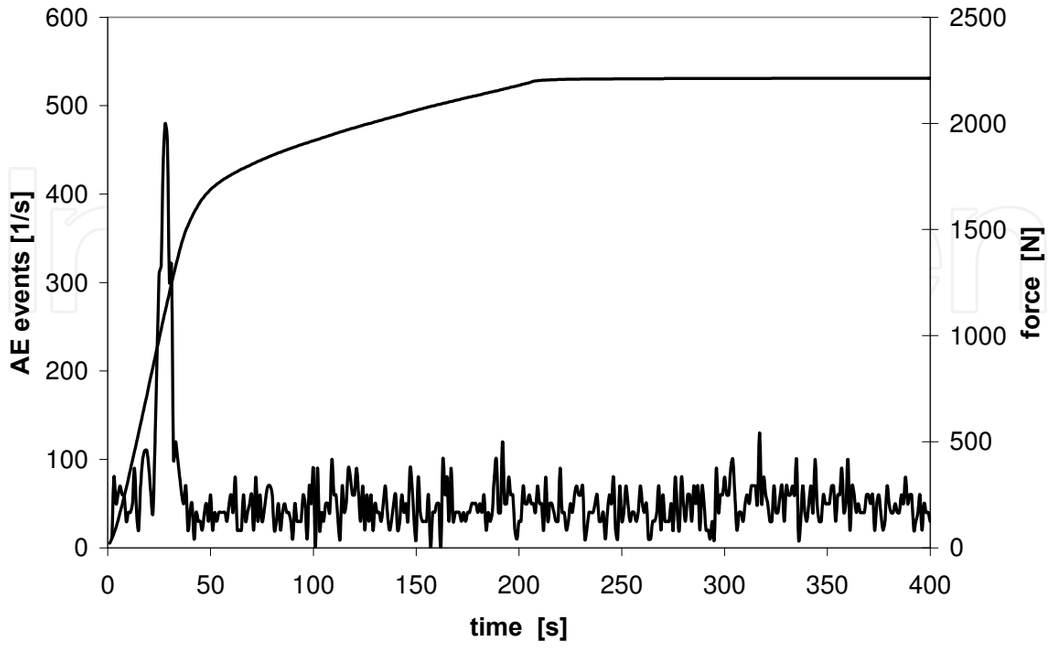

(a)

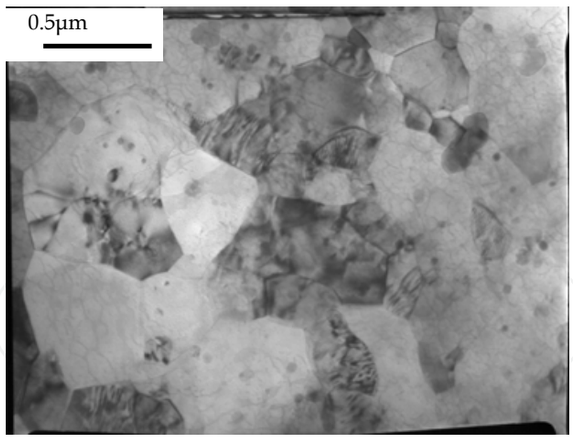

(b)

Fig. 19. Courses of AE and compressive force (a) in AA2014 Al alloy compressed after 2-fold ECAP processing of circular cross section and its corresponding TEM microstructure (b)

4.2 AE in Al AA6060 and AA2014 alloys compressed before and after HPT treatment

The AE and compressive force courses were examined on the Al AA6060 alloys subjected to compression tests before the HPT operation, after one and two HPT operations (Figs. 20a and 20b, respectively). It is visible, that the AE distinctly decreases after two-fold HPT processing compared with the AE level after one HTP operation. However, from Fig. 21, an evident decrease of the AE rate in the sample already after one HPT rotation (Fig. 21b) compared with the initial state of AA2014 alloy sample (Fig. 21a) can be observed.

4.3 Comparison to Mg-Li and Mg-Li-Al alloys

Fig. 22 presents one of more important results obtained so far on the Mg8Li alloy compressed before and after the application of ECAP technique in squared cross section channel (Kuśnierz et al., 2008). These results are even more pronounced in the case of Mg10Li and Mg10Li5Al alloys compressed after the application of HPT technique (Kúdela et al., 2011). The result of the applied HPT process, is presented in Fig. 23 for the Mg10Li alloy after a three-fold, whereas the relation of AE activity versus compression force for the Mg10Li5Al alloy is shown in Fig. 24 also after a three-fold HPT treatment.

The decrease of AE activity of compressed samples subjected to the both ECAP and HPT processes is closely connected with the size of grains. The initial microstructure of Mg8Li alloys (Fig. 22a) consists of size grains of order of several hundreds of micrometers (10^2µm), whereas the microstructure after a large plastic deformation by ECAP is visible in Fig. 22b. After the ECAP and/or HPT processes, applying only a few rotations, the grain size decreased three orders of magnitude to hundreds of nanometers (10^{-1}µm, Fig. 22b, 23b and 24b). These microstructures of Mg-Li and Mg-Li-Al alloys, presented in are the most pronounced examples of the refining effect of intensive strain processes arriving at UFG and/or nanocrystalline structure.

On the other hand the decrease of the AE level in Mg10Li and Mg10Li5Al (Figs. 23a and 24a) is of about two order of magnitude, as in the case before HPT operation, not presented here, since it is about 10^4/s, similarly as in the case of Mg8Li alloys (Fig. 22a).

The similar statement we can refer to the microstructures of Al alloys of AA6060 and AA2014 type, presented in Figs. 18 and 19, respectively. The phenomenon of the decrease of

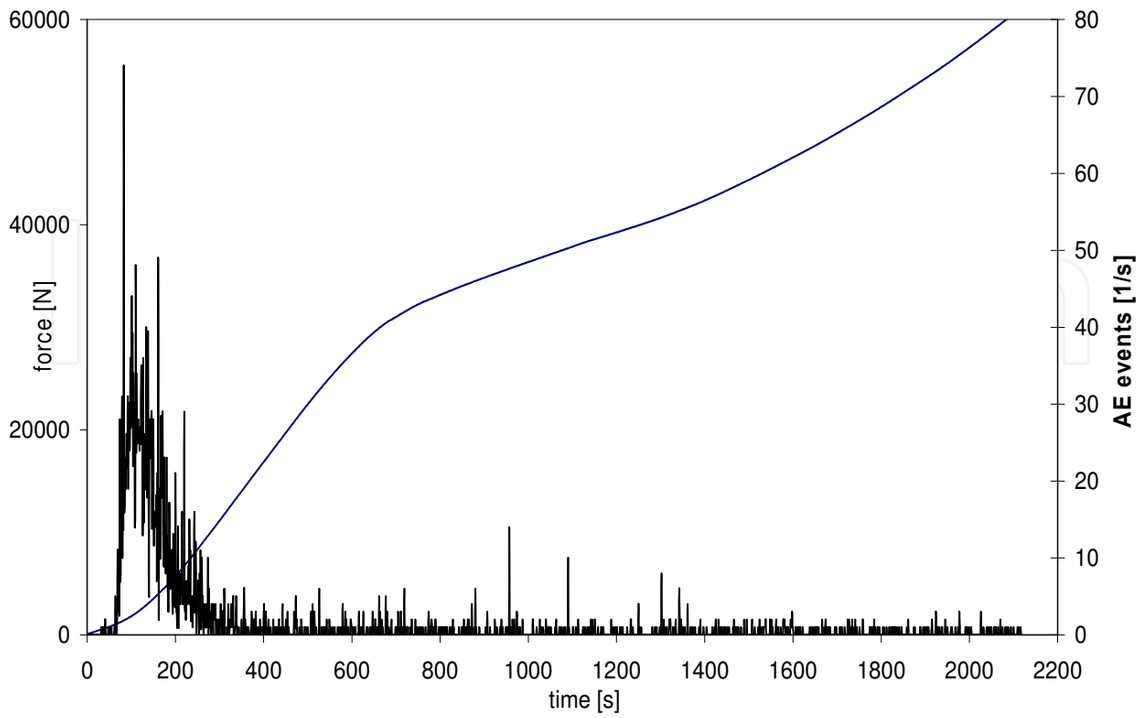

(a)

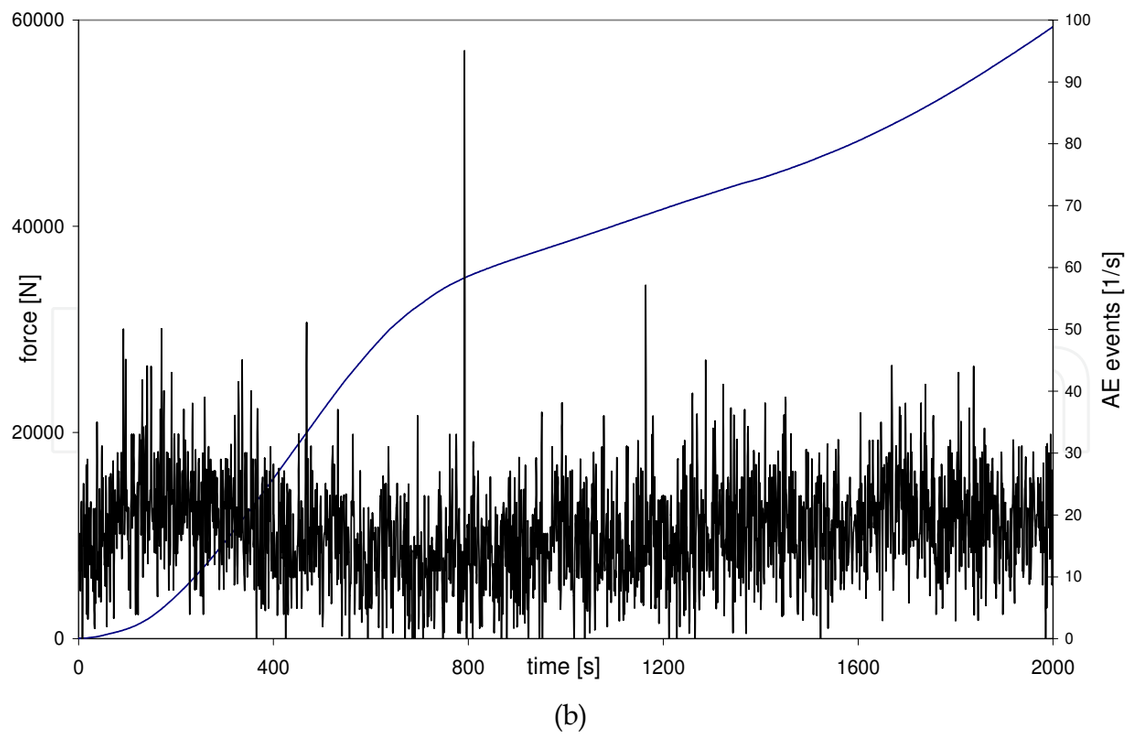

(b)

Fig. 20. AE and compressive force in dependence on time in Al alloy of AA6060 type subjected to tests of compression after one (a) and two (b) HPT processes

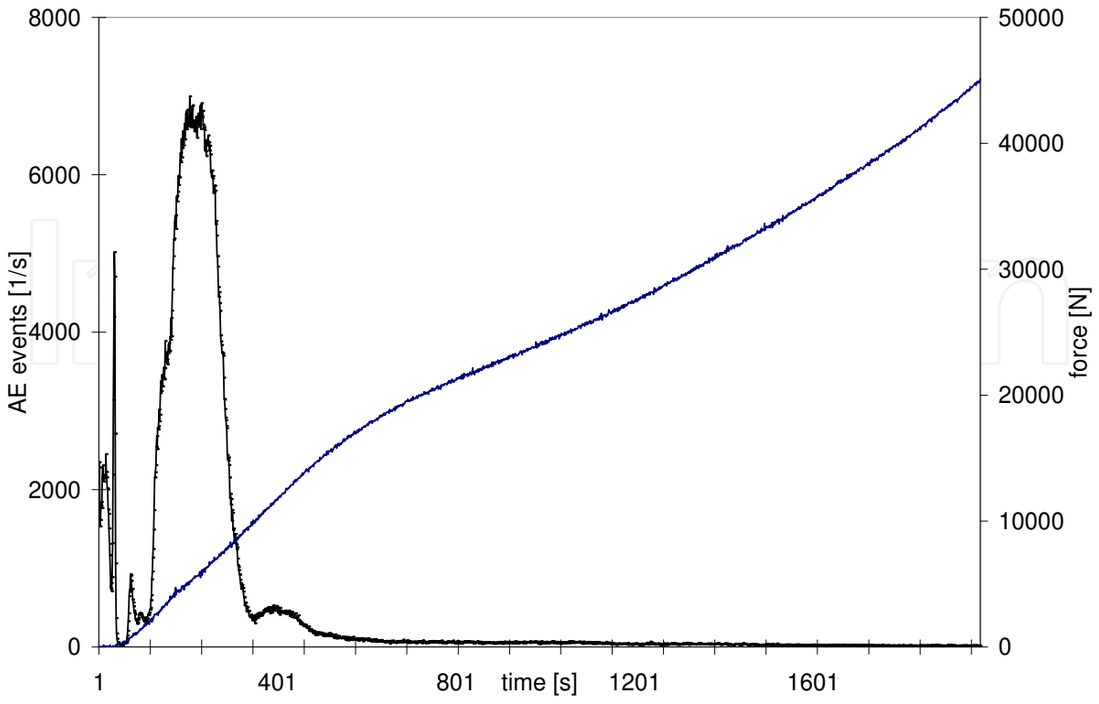

(a)

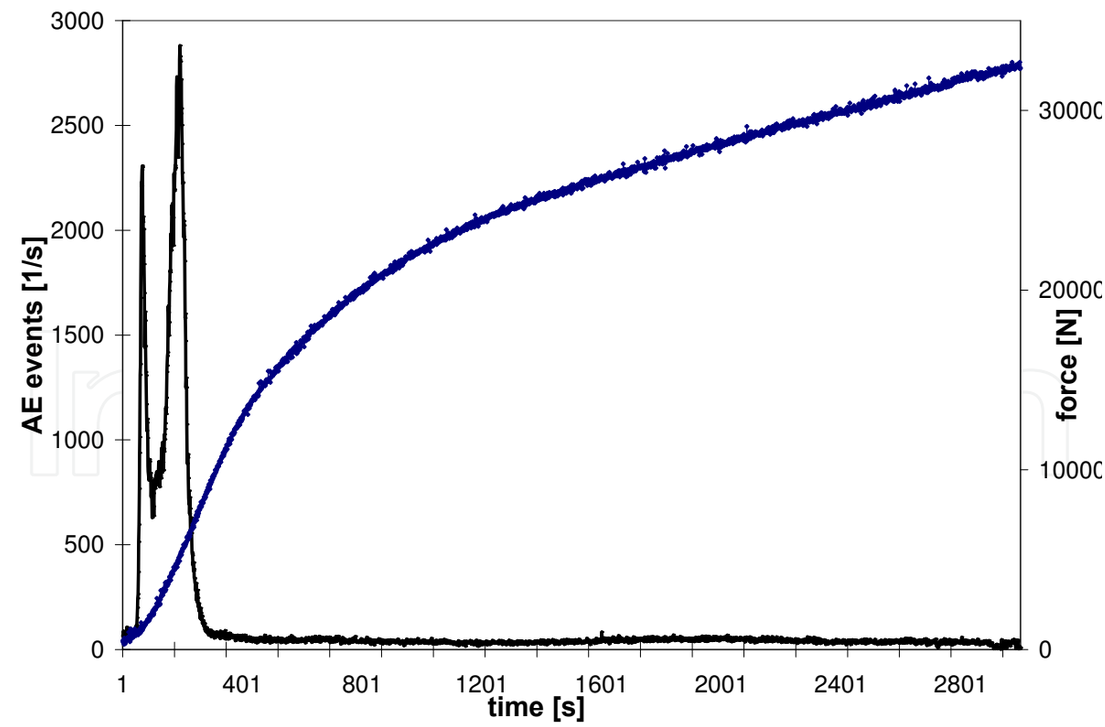

(b)

Fig. 21. Behavior of AE and compressive force in dependence on time in Al alloy of AA2014 type subjected to tests of compression before (a) and after one HPT process (b)

intensity and activity of AE in the materials subjected to intensive strain processing, may be explained here based on the consideration of two vital processes. The first one is connected with the strengthening mechanism resulting from the intensive deformation, because a significant growth of dislocation density compared with the initial state takes place after the processing. In this way a collective motion of dislocations generated during the compression is strongly limited due to intensive interaction of mobile dislocations, e.g. with the forest dislocations or precipitate particles and solute atoms. Another process is bound with the tendency to the growth of plasticity (or even superplasticity) in intensively deformed materials. The contribution in the AE decrease after the intensive processing occurs, when on the expense of typical dislocation slips along the favored planes of the crystalline lattice within individual grains, the start of the grain boundary slips begins, which is probably less acoustically effective compared with the effective mechanism of collective and synchronized annihilation of many dislocations.

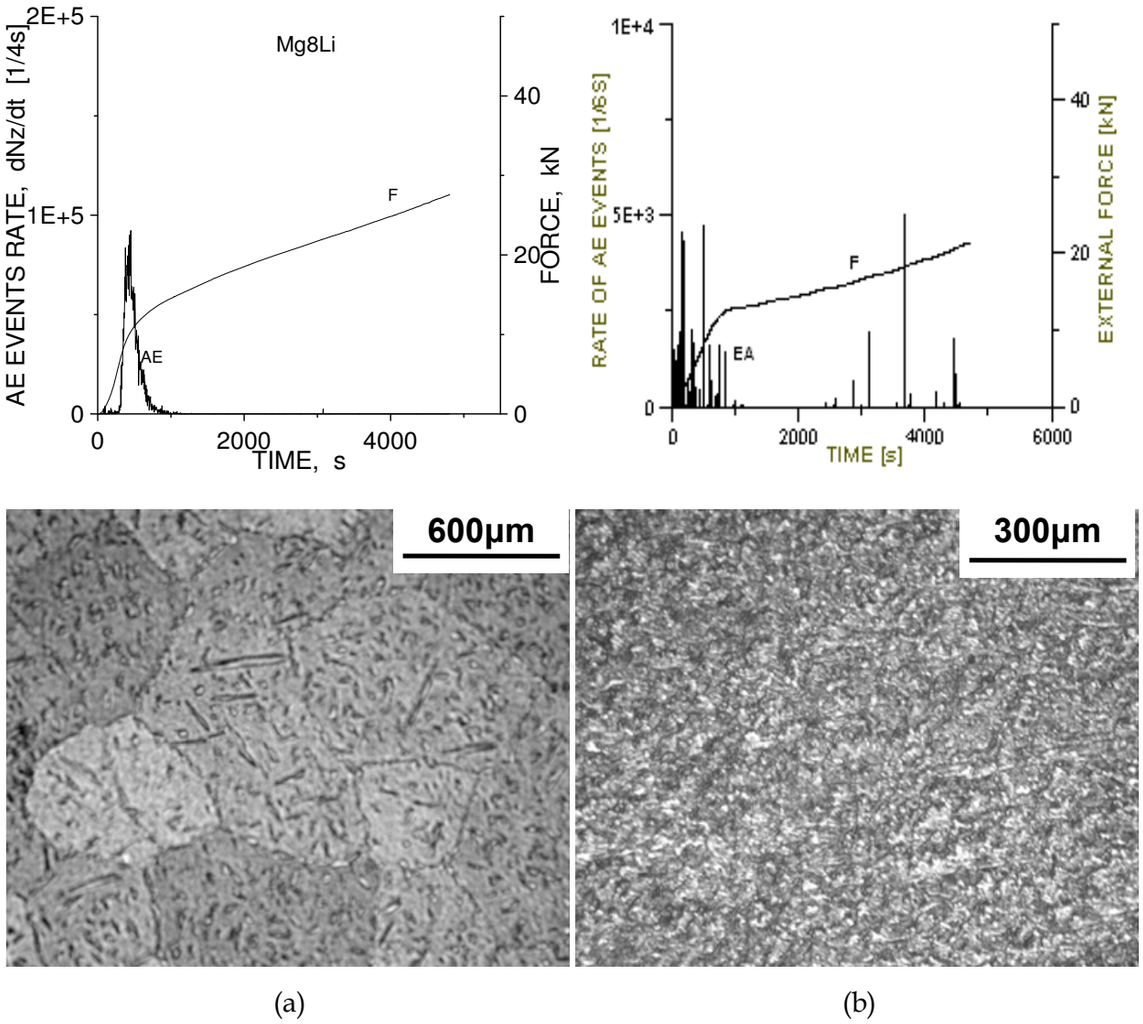

(a) (b)

Fig. 22. AE and external force in two-phase Mg8Li alloys before (a) and after (b) four-fold ECAP processing. At the bottom the corresponding optical microstructures

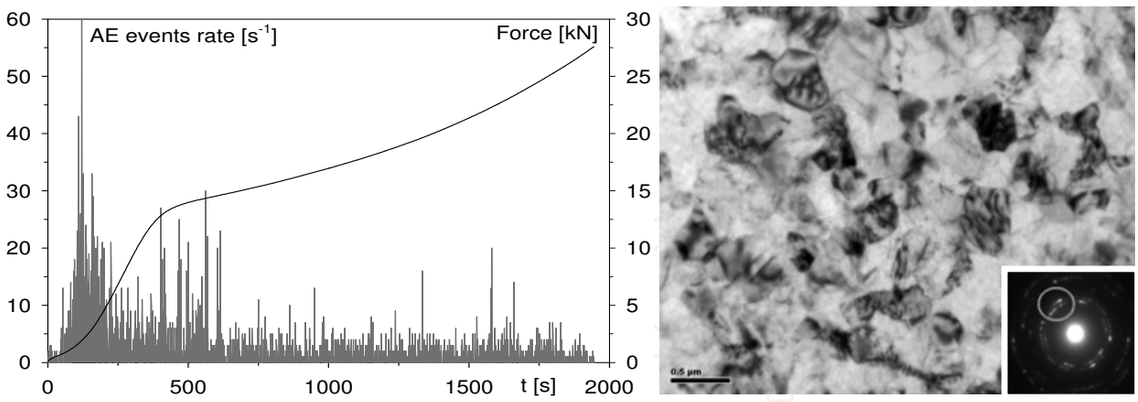

(a) (b)

Fig. 23. Courses of AE events rate and force versus time during compression of Mg10Li alloy after application of three-fold HPT rotations (a) and corresponding TEM microstructure (b)

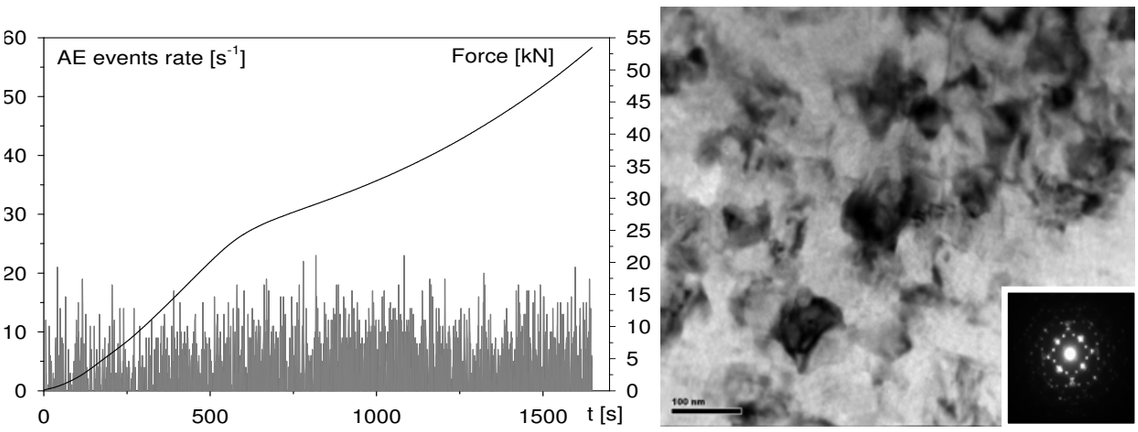

(a) (b)

Fig. 24. Courses of AE events rate and force versus time during compression of Mg10Li5Al alloy after three-fold HPT operation (a) and corresponding TEM microstructure (b)

4.4 AE and the Portevin–Le Châtelier effects in Al alloys

The AE effect, which accompany the Portevin–Le Châtelier one (PL effect – known also as discontinuous or serrated yielding or jerky flow), are quite well documented (van den Beukel, 1980; Caceres & Bertorello, 1983; Cottrell, 1953; Korbel et al., 1976; Pascual, 1974; Pawełek, 1989). Pascual (Pascual, 1974), as one of the first showed, that strong correlations occurred between the AE behavior and plastic flow instabilities, resulting from the in-homogenous deformation are typical for the PL phenomenon.

It was established that the local peaks of yielding corresponded to the increases of AE and that they resulted from the dislocation breakaway from the atmospheres of foreign atoms (Cottrell atmospheres) as well as the multiplication of dislocations at the front of propagating deformation band, similar to the well known Lüders' band. The results presented below will be shortly discussed further on the basis of a simple dislocation-dynamic (DD) model of PL effect (Pawełek, 1989), described slightly in section 4.4.2.

4.4.1 Anisotropy of AE and PL effects in Al alloys

The phenomenon of PL effect anisotropy was observed for the first time in works (Mizera & Kurzydłowski, 2001; Pawełek et al., 1998). The present research was carried out in order to confirm the anisotropy of the both AE and PL phenomena as well as to study the possibility of the occurrence of PL and/or AE effects also in materials processed with intensive deformation techniques (Pawełek et al., 2007, 2009).

Al alloys of AA5754 type. The examinations of PL and AE effects were performed in fact for 5 orientations of samples cut out at angles β=0°, 22.5°, 45°, 67.5° and 90° with respect to the rolling direction. Fig. 25, shows the AE rate and courses of external force during the tensile tests only for three samples of Al alloys of AA5754 type.

orientation (cut out angle *β)*	0°	22.5°	45°	67.5°	90°
total number of events Σ_C for AA5754 alloy	3400	3500	8020	2520	4500

Table 1. The total sum of AE events in Al AA5754 alloy in dependence on cut out angle β

Moreover, when analyzing the plots in Fig. 25a-c, it can be found, that anisotropy of AE in AA5754 alloy is connected with the maximum quantities Σ_c (about 8000), which occur for cut out angles β=45° whereas the minimum of Σ_c (about 2500) is for β=67.5°. It is illustrated in Table 1, where maximum Σ_c (red color) and minimum ones (blue) are given.

Al alloys of AA5182 type. Cold rolled sheets of Al AA5182 alloy were the subject of plastic deformation anisotropy analysis connected with the PL effect. The samples were cut out of the rolled sheet along the rolling direction (RD), transverse direction (TD) and at angle 45° between them. The investigated sheets were subjected to uniaxial tension at ambient temperature using a static QTEST testing machine at constant strain rate $5.3 \times 10^{-4} s^{-1}$ to the moment of their failure. In Fig. 26, the corresponding collection of intensity of AE signal counts recorded during the tensile test are showed in the form of histogram.

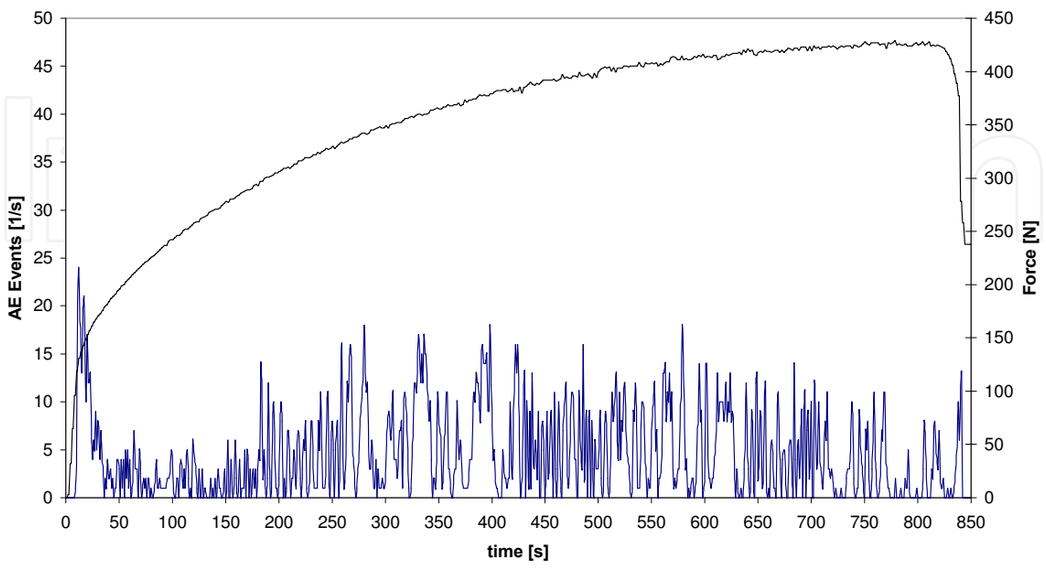

(a)

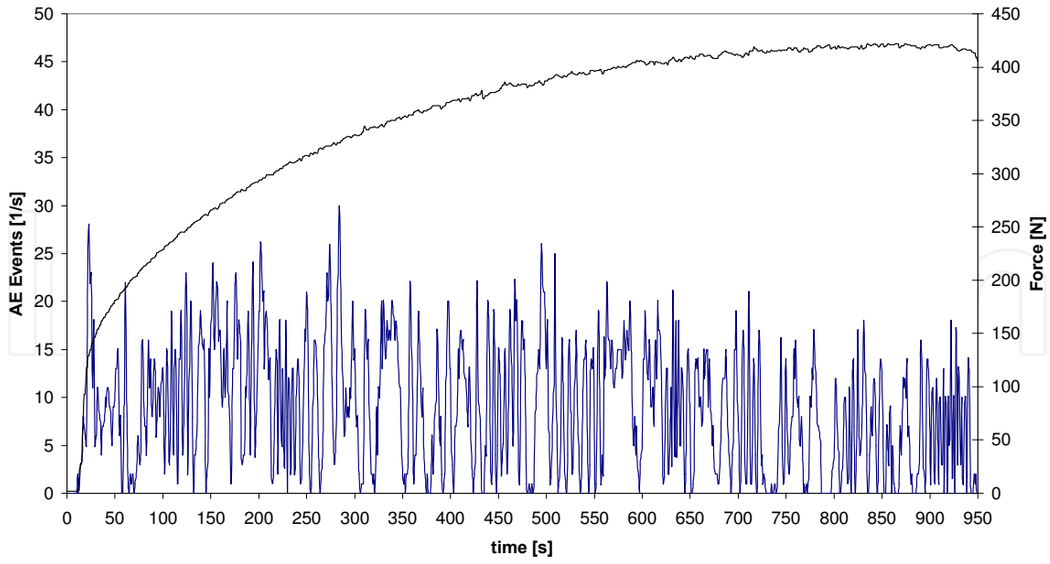

(b)

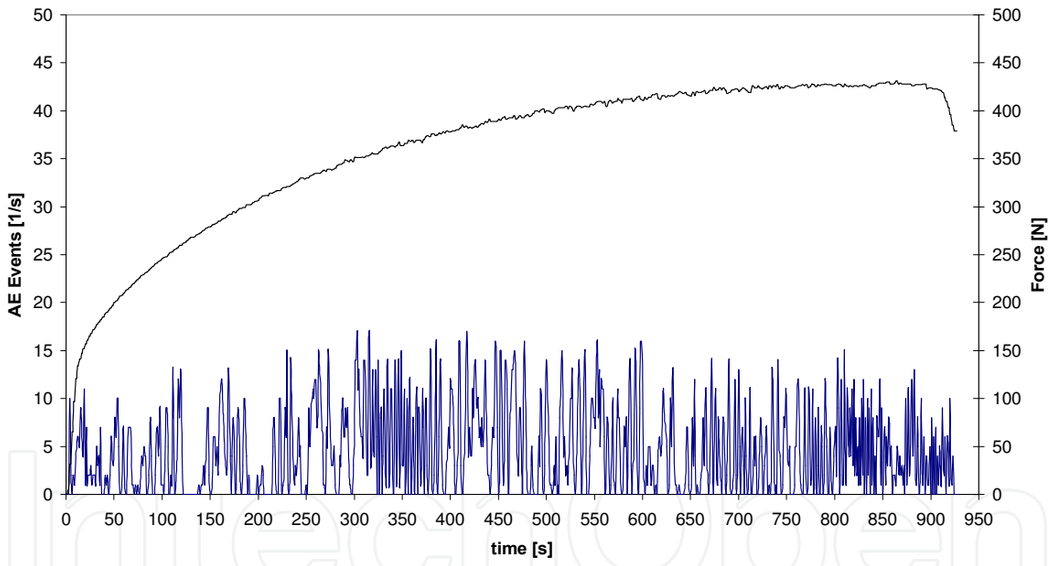

(c)

Fig. 25. Anisotropy of AE and PL effects in tensile test of Al AA5754 alloy. AE and external force for individual cut out angles: (a) – β=0°, (b) – β=45° and (c) – β=90°

The anisotropy of PL and AE effects in these alloys resulted from the fact, that the highest number of AE signal counts were recorded during the tension of samples, which were cut out in the TD direction perpendicular to the rolling direction RD.

The correlations of amplitude of AE signals with the tensile curves of samples in the rolling direction, transverse direction and inclined 45° to them are shown in Fig. 27. The analysis of the results showed that during plastic deformation of the Al AA5182 alloy the AE intensity bound with the motion of dislocation occurs at a defined level of load dependant on

microstructure of materials. As it was suggested in previous works (Pawełek et al., 1998) the different distribution of grain orientations, i.e. the differentiation of sample textures were found to be reasons for the anisotropy of AE and PL. Generally, it means that the maximum AE, for example in the Al AA5754 sample for β=45°, is the result of the fact that the number of privileged slip systems of {111} type is greater than in the sample for other values of β, and, in consequence the number of active dislocation sources generating the AE events is greater. Moreover, the reasons for the AE generation during the effect of PL are related with the collective behavior of dislocation groups generated by the sources formerly blocked by the Cottrell atmospheres. Based on Cottrell idea, an own model of PL effect was proposed in (Pawełek, 1989). This model is presented schematically in Fig. 30 and discussed in short in the next section.

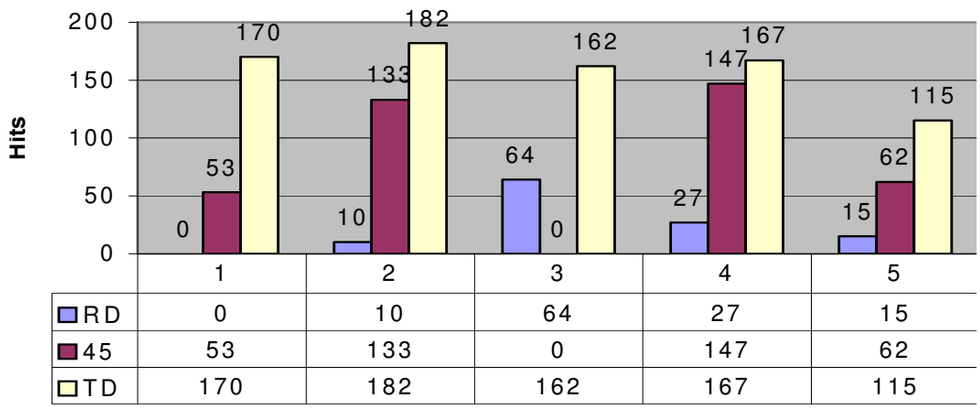

	1	2	3	4	5
RD	0	10	64	27	15
45	53	133	0	147	62
TD	170	182	162	167	115

Fig. 26. Intensities of AE signals during tensile test in the form of histogram

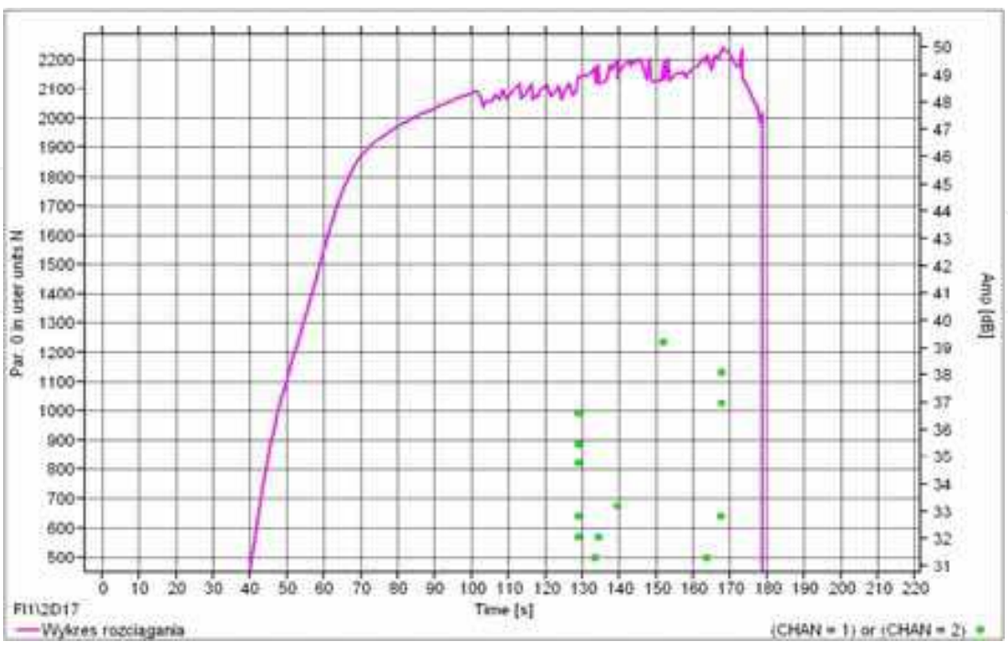

(a)

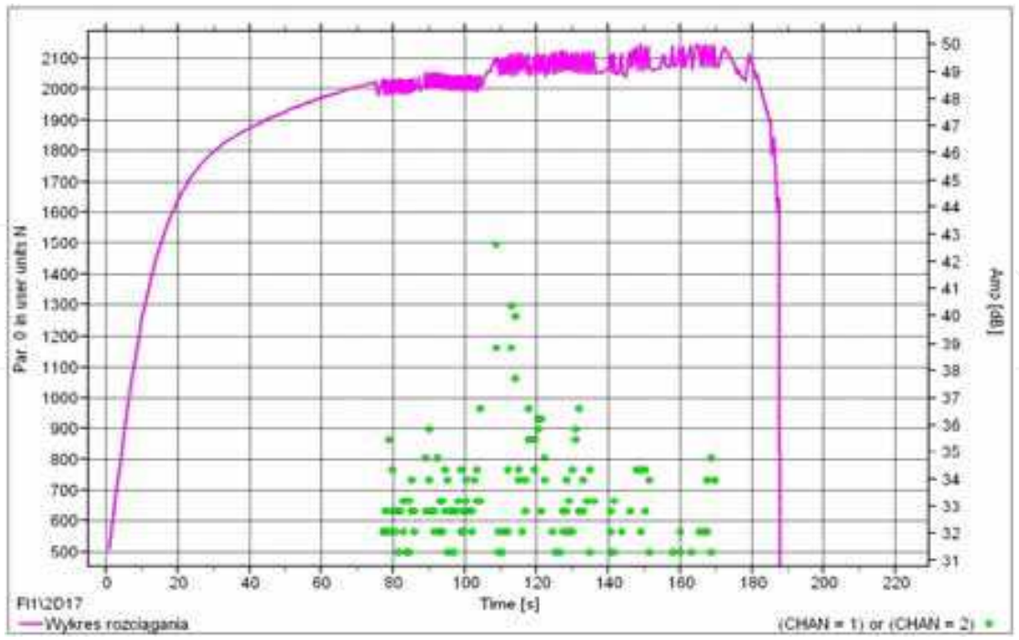

(b)

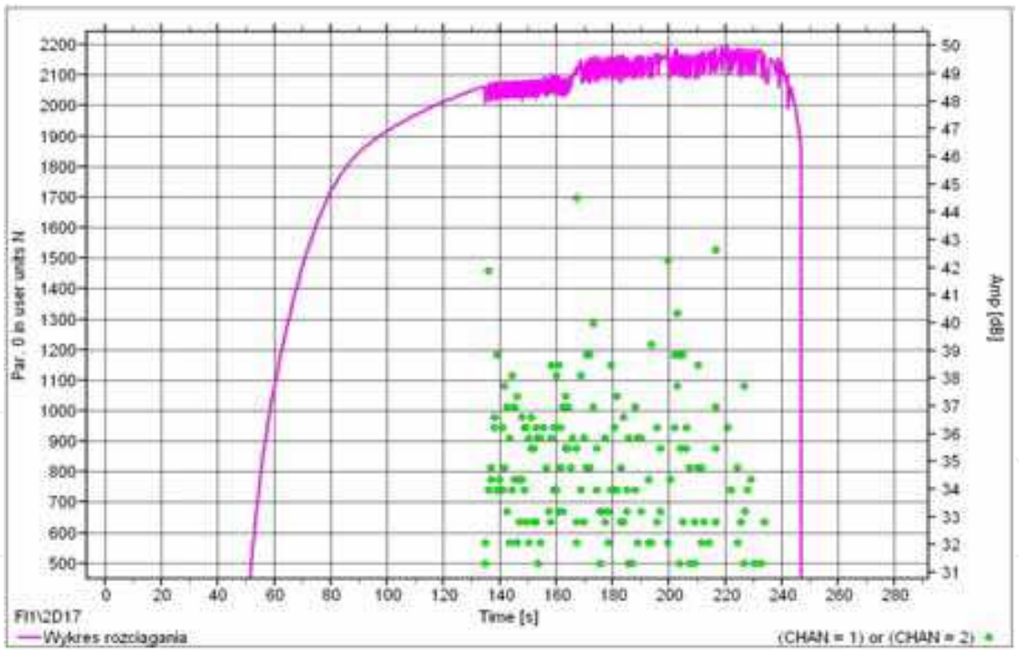

(c)

Fig. 27. Correlations of amplitude of AE signals with the tension curve of samples in the rolling direction (a); transverse direction (b) and inclined 45° to them (c)

4.4.2 AE and PL effects in Al AA5251 alloys processed with the ARB method

The results of the first investigations of the relations between the mechanical properties, PL effect and the AE signals generated in a tensile test of Al alloys of AA5251 type before and

after ARB process are presented in Fig. 28. It is shown that in the case of not pre-deformed alloy (Fig. 28a) more essential correlations between the AE and the PL effects appear than in the case of alloy, pre-deformed with the ARB method (Fig. 28b). The behavior of force and AE during tension of AA5251 alloy obtained after n=6 passes of ARB. It can be seen that the correlations between the PL and AE effects continue to occur: local drops of force, characteristic for the PL effect correspond to the peaks of the rate of AE events. However, both the activity and the intensity of AE as well as the values of the local drops of force are no longer so distinct as in the case of not pre-deformed samples. Thus, it can be said that both the PL and the AE effects in samples of more refined grain size (UFG, nanocrystalline) show the tendency to disappear.

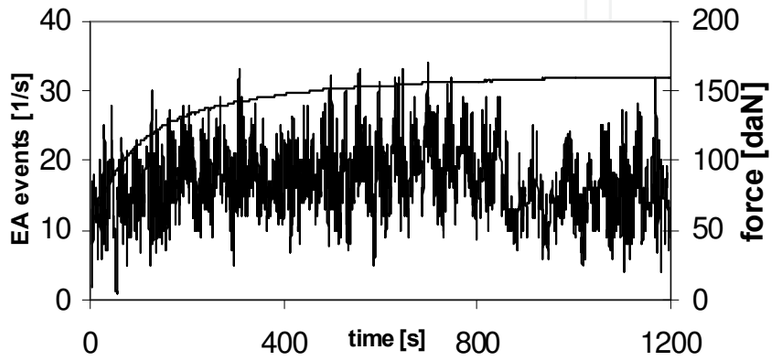

(a)

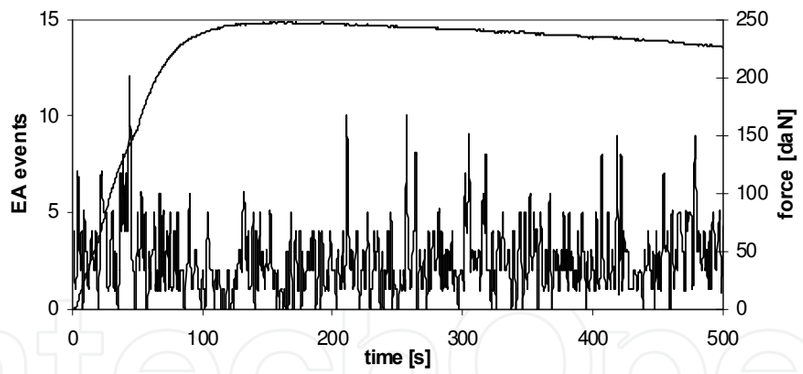

(b)

Fig. 28. Correlations between the AE behavior and the course of force during the PL effect in a tensile test of AA5251 alloy before (a) and after (b) the application of ARB operation

The application of modern software enabled the spectral analysis of AE signals in the preparation of acoustic maps (acoustograms). Fig. 29 shows, by the way of example, such an acoustogram for a sample after n=6 passes by the ARB method. It should be especially noticed that it is clearly shown here that the correlations between the PL and AE effects occur in the frequency range of AE signals above 17kHz (except the line at about 360s), which seems to be a very characteristic, never noticed earlier, feature of the PL effect. In all cases where AE and PL effects were examined in not pre-deformed state, this frequency range was considerably lower – most often below 8 kHz.

Most of the models of PL effect (e.g. van den Beukel, 1980; Král & Lukáč, 1997; Onodera et al., 1997) are of phenomenological character and none of them explain clearly the physical mechanisms of the formation and propagation of the related deformation bands and which would be coherent with the models of the sources of AE. The presented results are briefly discussed below in the context of the dislocation models of the PL effect reported in literature (e.g. Pawełek, 1989; Pascual, 1974) and the theoretical concepts concerning the source of AE generation during plastic deformation of metals (e.g. Kosevich, 1979; Natsik & Burkhanov, 1972; Natsik & Chishko, 1972, 1975; Pawełek, 1988a; Pawełek et al., 2001).

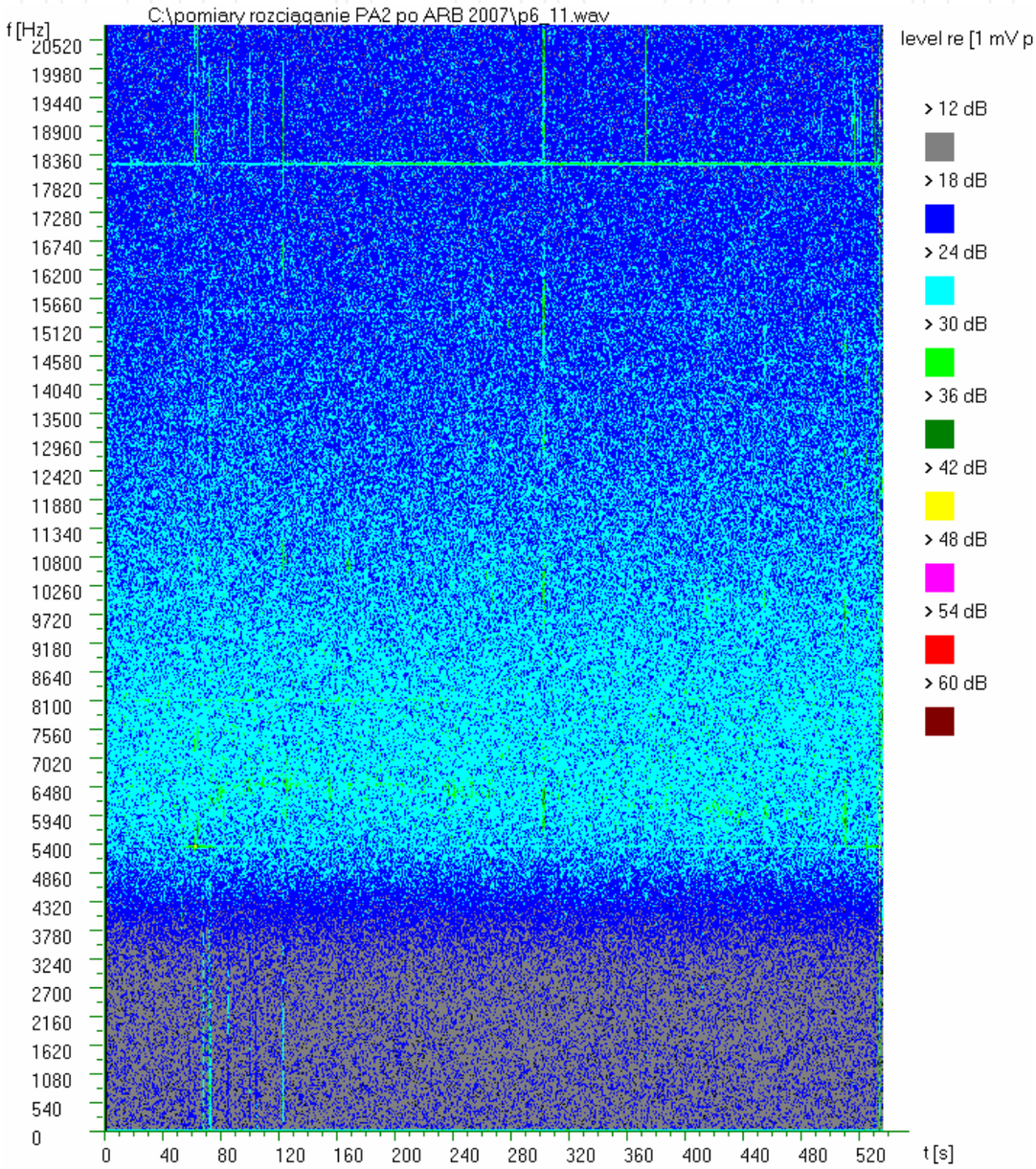

Fig. 29. Acoustic map of AE signals generated during PL effect in tensile test of AA5251 alloy after six repetitions of ARB operation

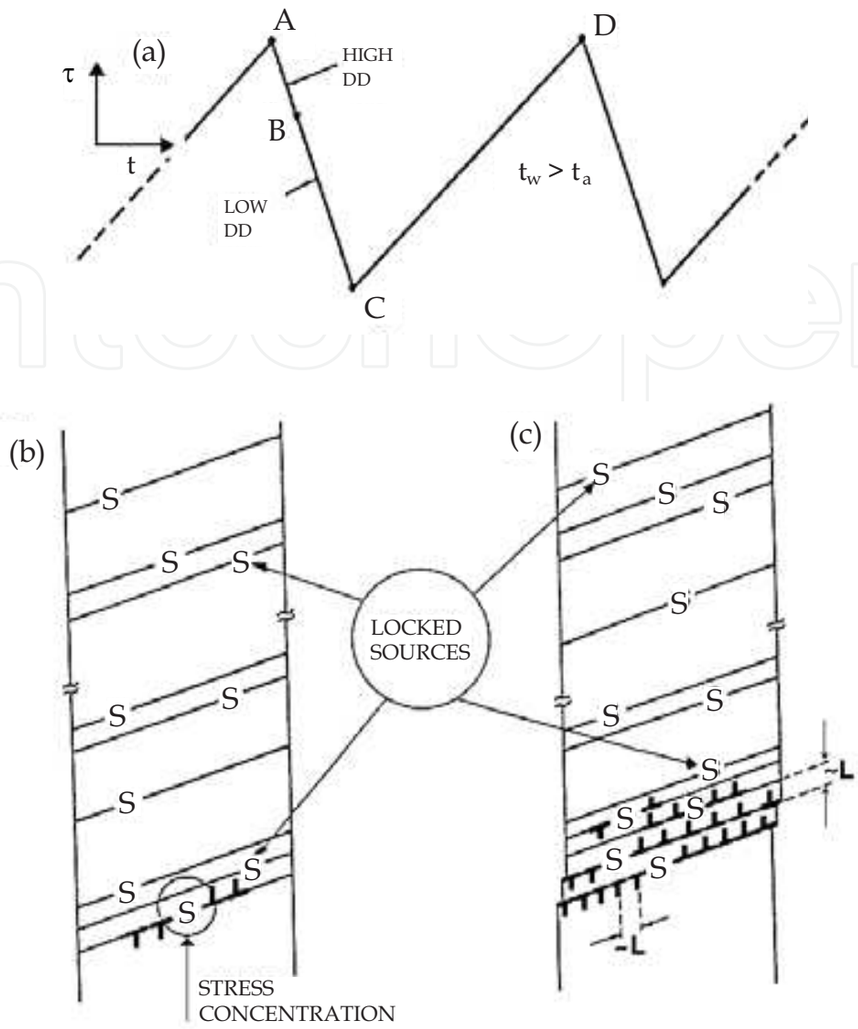

Fig. 30. Simple dislocation-dynamic (DD) model of the PL effect: (a) jump-like drop of force, (b) localization and nucleation of a band and (c) propagation of a slip band

In accordance with a simple dislocation-dynamic (DD) model of the PL effect (Pawełek, 1989), each local drop of the external force on the work-hardening curve (Fig. 30a) is connected with unlocking of the dislocation sources in a certain localized area of the sample. The consequence is the formation of a slip band (Fig. 30b) which continues to propagate (Fig. 30c) until the waiting time t_w reaches again the value of the aging time t_a. The strain rate in the slip band $\dot{\varepsilon}_d$ is greater than the rate of the homogeneous strain $\dot{\varepsilon}$ due the high DD. Accordingly, on force-time curve a local drop must occur (Fig. 30a), since, according to the known equation of Penning: $K^{-1}d\sigma/dt+\dot{\varepsilon}_d=\dot{\varepsilon}$ there occurs relation $d\sigma/dt<0$ for $\dot{\varepsilon}_d>\dot{\varepsilon}$; K is the coefficient of rigidity of the system of machine–sample.

The discussion was carried out in respect with collective properties of motion of many dislocation groups as well as the internal and surface synchronized annihilation of dislocations. The dislocation model of AE event generation was the starting point, which was based on soliton properties of dislocations (Pawełek, 1985, 1987, 1988a,b; Pawełek & Jaworski, 1988; Pawełek et al., 2001).

It was suggested, that the AE increases accompanying the local flow peaks were bound to highly dynamic sources of overstress, which acted in the state of strong overstress (Pawełek et al., 1985) due to an abrupt breakaway from the Cottrell atmospheres. It is thus very probable, that in this case, apart from the annihilation of dislocations, the contribution of the enhancement of dislocation dynamics, which, due to the effect of overstress of the dislocation sources (e.g. Frank-Read (FR) type), may be significantly higher that in the case of usual action of FR sources. Also the results of one of the latest works on the PL and AE effects (Chmelík et al., 1993) do confirm that the dominating factors binding both AE and PL phenomena result from the multiplication of dislocations during the action of FR sources and the breakaway of dislocations from the Cottrell atmospheres.
Simultaneously with the above process there takes place the generation of AE events both due to the acceleration as well as annihilation of dislocations. Dislocations generated from the FR sources may attain very great accelerations resulting from the interactions of the dislocation-dislocation type. However, there are more premises (Boiko et al., 1973, 1974, 1975) maintain that the contribution to AE signals due to annihilation is considerably higher than that resulting from acceleration. These authors carried out the calculations showing that the expression for AE included three terms related to the dislocation annihilation, the rate of dislocation generation and to the dislocation acceleration. However, at the same time the two last terms are always considerably less important than the dislocation annihilation term. Moreover, the contribution from the annihilation of the dislocation segments when the dislocation loops are bearing off from the FR source is intensified and dominated by the processes of the surface annihilation of dislocations, such as it takes place e.g. in the case of the formation of dislocation steps on the sample surface due to the formation of slip lines and slip bands or the shear microbands. This observation is in accordance with the results obtained in another work (Merson et al., 1997), in which the strong influence of the surface on the AE generated due to plastic deformation of metals was clearly demonstrated. Moreover, the anisotropy occurrence of PL and AE effects was confirmed on the example of AA5754 and AA5182 type of Al alloys. The tendency to the decrease of intensity of the AE and PL effects in UFG (nanocrystalline) Al alloy of AA5251 type was observed (Pawełek, 2009) for the first time.

5. Conclusions

The more important results obtained in this chapter may be formulated in the form of the following, more detailed conclusions:

- The AE method shows, that low temperature transition of the twinning → shear bands observed in Cu and Ag single crystals is also observed in Al single crystals.
- The formation of an individual twin lamella, a micro shear band and step on the surface is related with the generation of AE peak due to surface annihilation of $10^4 \div 10^6$ dislocations.
- The intensity and activity of AE in alloys subjected to compression tests after processing with the methods of intensive deformation (HPT, ECAP and ARB) distinctly fell in respect to the unprocessed alloys.
- The decrease of AE in intensively processed alloys is connected with a significant increase of refinement of microstructure and the tendency to the plasticity growth.

- The correlations between the AE and the mechanisms of deformation may be considered in terms of collective synchronized acceleration and annihilation of many dislocations.
- A hypothesis, that the decrease of AE in alloys compressed after intensive strain is due to strengthening processes and beginning of slip along grain boundaries was put forward.
- The anisotropy of AE and PL effects is bound with the maximum value of total sum of AE events and maximum abrupt drops of external force.
- The PL and AE effects in alloy after ARB treatment reveal the tendency to disappear.
- The relation of AE and PL effects is in good accordance with a simplified dislocation-dynamic model of the PL phenomenon.
- Correlations between the PL and AE effects occur in the frequency range above 17kHz, whereas in metals, not generating the PL effect, they occur in a lower range – below 8kHz.

6. Acknowledgement

The studies were financially supported by the research projects of the Polish Ministry of Science and Higher Education No N N507 598038 and No N507 056 31/128 as well as by the research project of the Polish Committee for Scientific Research No 3 T08A 032 28.
I would like to thank also my friends and coworkers: dr Andrzej Piątkowski, prof. Zbigniew Ranachowski, dr Stanislav Kúdela, prof. Henryk Paul and prof. Zdzisław Jasieński, for their contribution to the presented paper and valuable discussion.

7. References

Beukel, van den, A. (1975). Theory of the Effect of Dynamic Strain Aging on Mechanical Properties. *Physica Status Solidi A*, Vol.30, pp.197-206, ISSN 0031-8965.

Bidlingmaier, T.; Wanner, A.; Dehm, G. & Clemens H. (1999). Acoustic Emission during Room Temperature Deformation of a γ-TiAl Based Alloy. *Zeitschrift für Metallkunde,* Vol.90, No.8, pp.581-587, ISSN 0044-3093.

Boiko, V.S. (1973). Dislocation Description of Twin Dynamic Behavior. *Physica Status Solidi B*, Vol.55, pp.477- 482, ISSN 0370-1972.

Boiko, V.S.; Garber, R.I.; Krivenko, L.F. & Krivulya, S.S. (1973). *Fiz. tverd. Tela,* Vol.15, p.321.

Boiko, V.S.; Garber, R.I. & Krivenko, L.F. (1974). *Fiz. tverd. Tela,* Vol.16, p.1233.

Boiko, V.S.; Garber, R.I.; Kivshik, V.F. & Krivenko L.F. (1975). *Fiz. tverd. Tela,* Vol.17, p.1541.

Caceres, C.H. & Bertorello H.R. (1983). Acoustic emission during non-homogeneous flow in Al Mg alloys. *Scripta Metallurgica,* Vol.17, No.9, pp.1115-1120.

Cottrell, A.H. (1958). Dislocations and Plastic Flow in Crystals, Oxford University Press.

Chmelík, F.; Trojanowá, Z.; Převorovský, Z. & Lukáč P. (1993). The Portevin-Le Châtelier effect in Al-2.92%Mg-0.38%Mn alloy and linear location of acoustic emission. *Materials Science & Engineering A,* Vol.164, Nos.1-2, (May 1993), pp.260-265, ISSN 0921-5093.

El-Danaf, E.; Kalidindi, S.R. & Doherty, R.D. (1999). Influence of Grain Size and Stacking-Fault Energy on Deformation Twinning in Fcc Metals. *Metallurgical and Materials Transactions A,* Vol.30, (May 1999), pp.1223-1233, ISSN 1073-5623.

Heiple, C.R. & Carpenter, S.H. (1987). *Journal of Acoustic Emission,* Vol.3, p.177.

Jasieński, Z.; Pawełek, A. & Piątkowski, A. (2010). Low temperature deformation twinning in channel-die compressed aluminium single crystals evidenced by acoustic emission. *Materials Science-Poland*, Vol.31, No.3, pp.528-530, ISSN 0208-6247.

Kuśnierz, J. (2001). Microstructure and texture evolving under Equal Channel Angular (ECA) processing. *Archives of Metallurgy,* Vol.46, No.4, pp.375-384, ISSN 0860-7052.

Kúdela, S.; Pawełek, A.; Ranachowski, Z.; Piątkowski, A.; Kúdela, S., Jr. & Ranachowski, P. (2011). Effect of Al alloying on the Hall-Petch strengthening and Acoustic Emission in compressed Mg-Li-Al Alloys after HPT processing. *Kovové Materiály – Metallic Materials,* Vol.49, No.4, pp.271-277, ISSN 0023-432X.

Kuśnierz, J.; Pawełek, A.; Ranachowski, Z.; Piątkowski, A.; Jasieński, Z.; Kudela, S. & Kudela, S., Jr. (2008). Mechanical and Acoustic Emission Behavior Induced by Channel-Die Compression of Mg-Li Nanocrystalline Alloys Obtained by ECAP Technique. *Reviews on Advanced Materials Science,* Vol.18, pp.583-589,

Korbel, A.; Zasadziński J. & Sieklucka Z. (1976). A new approach to the Portevin-LeChatelier effect. *Acta Meallurgica,* Vol.24, No.10, (October 1976), pp.919-923, ISSN 0001-6160.

Král, R. & Lukáč P. (1997). Modelling of strain hardening and its relation to the onset of Portevin-Le Chatelier effect in Al-Mg alloys. *Materials Science & Engineering A,* Vol. 234-236, pp.786-789, ISSN 0921-5093.

Kosevich, A.M. (1979). In: *Dislocations in Solids,* F.R.N. Nabarro, (Ed.), Vol.1, p.33, North-Holland Publ. Co., Amsterdam, The Netherlands.

Mizera, K. & Kurzydłowski, K.J. (2001). On the anisotropy of the Portevin-Le Chatelier plastic instabilities in Al-Li-Cu-Zr alloy. *Scripta Materialia,* Vol.45, No.7, (October 2001), pp.801-806, ISSN 1359-6462.

Merson, D.; Nadtochiy, M.; Patlan, V.; Vinogradov, A. & Kitagawa, K. (1997). On the role of free surface in acoustic emission. *Materials Science & Engineering A,* Vol.234-236, pp.587-590, ISSN 0921-5093.

Natsik, W.D. & Burkhanov, A.N. (1972). *Fiz. tverd. Tela,* Vol.14, p.1289.

Natsik, W.D. & Chishko, K.A. (1972). *Fiz. tverd. Tela,*Vol.15, p.3126; (1975). ibid, Vol.17, p.341.

Onodera, R.; Morikawa, T. & Higushida, K. (1997). Computer simulation of Portevin-Le Chatelier effect based on strain softening model. *Materials Science & Engineering A,* Vol.234-236, pp.533-536, ISSN 0921-5093.

Paupolis, A. (1980). *Circuits and Systems. A Modern Approach,* Holt, Rinehart & Winston, (Ed.), New York, USA.

Pawełek, A.; Piątkowski, A. & Jasieński, Z. (1997). Nonlinear and dislocation dynamic aspects of acoustic emission and microstructure evolution during channel-die compression of metals. *Molecular and Quantum Acoustics,* Vol.18, 321-358, ISSN 0208-5151.

Pawełek, A.; Piątkowski, A.; Jasieński, Z. & Pilecki S. (2001). Acoustic Emission and Strain Localization in FCC Single Crystals Compressed in Channel-Die at Low Temperature. *Zeitschrift für Metallkunde,* Vol.92, No.4, pp.376-381, ISSN 0044-3093.

Paul, H.; Darrieulat, M. & Piątkowski, A. (2001). Local Orientation Changes and Shear Bending in {112}<111>-Oriented Aluminium Single Crystals. *Zeitschrift für Metallkunde,* Vol.92, No.11, pp.1213-1221, ISSN 0044-3093.

Pascual, R. (1974). Acoustic emission and dislocation multiplication during serrated flow of an aluminium alloy. *Scripta metallurgica.,* Vol.8, No.12, pp.1461-1466.

Pawełek, A. (1989). On the Dislocation-Dynamic Theory of the Portevin-Le Chatelier Effect. *Zeitschrift für Metallkunde,* Vol.80, No.9, pp.614-618, ISSN 0044-3093.

Pawełek, A.; Piątkowski, A.; Jasieński, Z.; Litwora, A. & Paul, H. (1998). Acoustic emission and Portevin-Le Chatelier effect during tensile deformation of polycrystalline α-brass. *Molecular and Quantum Acoustics,* Vol.19, pp.201-215, ISSN 0208-5151.

Pawełek, A.; Kuśnierz, J.; Jasieński, Z.; Ranachowski, Z. & Bogucka, J. (2009). Acoustic emission and the Portevin – Le Châtelier effect in tensile tested Al alloys before and after processing by accumulative roll bonding (ARB) technique*, Proceeding of 10th French-Polish Colloquium*, Paris, France, May 20-21, 2008; *Archives of Metallurgy and Materials,* Vol.54, No.1, pp.83-88, ISSN 1733-3490.

Pawełek, A.; Bogucka, J.; Ranachowski, Z.; Kudela, S. & Kudela, S., Jr. (2007). Acoustic emission in compressed Mg-Li and Al alloys processed by ECAP, HPT and ARB methods. *Archives of Acoustics,* Vol.32, No.4 (Supplement), pp.87-93, ISSN 0137-5075.

Pawełek, A. (1988a). Possibility of a soliton description of acoustic emission during plastic deformation of crystals. *Journal of Applied Physics,* Vol.63, No.11, (June 1988), pp.5320-5325, ISSN 0021-8979.

Pawełek, A. (1988b). An attempt at a soliton approach to plastic flow of crystals. *Physics Letters A*, Vol.128, No.1,2, (March 1988), pp.61-65, ISSN 0375-9601.

Pawełek, A. (1987). Density of kiks on a dislocation segment in thermodynamic equilibrium and the interaction between solitons. *Journal of Applied Physics,* Vol.62, No.6, (September 1987), pp.2549-2550, ISSN 0021-8979.

Pawełek, A. & Jaworski, M. (1988). A moving dislocation kink as the soliton on a background of quasi periodic process in unbounded sine-Gordon system. *Journal of Applied Physics,* Vol.64, No.1, (July 1988), pp.119-122, ISSN 0021-8979.

Pawełek, A. (1985). Soliton-soliton and soliton-antisoliton interaction in the Frenkel-Kontorova model of dislocation. *Acta Physica Polonica A,* Vol.68, No.6 (December 1985), pp.815-831, ISSN 0587-4264.

Pawełek, A.; Stryjewski, W.; Bochniak, W. & Dybiec, H. (1985). Mobile Dislocation Density Variation during Strain Rate Change Evidenced by Acoustic Emission. *Physica Status Solidi A*, Vol.90, pp.531-536, ISSN 0031-8965.

Ranachowski, Z.; Piątkowski, A.; Pawełek, A. & Jasieński, Z. (2006). Spectral analysis of acoustic emission signals generated by twinning and shear band formation in silver single crystals subjected to channel-die compression tests. *Archives of Acoustics,* Vol.31, No.4 (Supplement), pp.91-97, ISSN 0137-5075.

Resnikoff, H. & Wells, R. (1998). *Wevelet Analysis*, Springer, New York, USA.

Saito, Y.; Utsunomiy, H.; Tsuji, A. N. & Sakai, T. (1999). Novel ultra-high straining process for bulk materials – development of the accumulative roll-bonding (ARB) process. *Acta Materialia,* Vol.47, No.2, (January 1999), pp.579-583, ISSN 1359-6454.

Scott, I. G. (1991).*Basic Acoustic Emission*, Gordon and Breach, New York, USA.

Tanaka, H. & Horiuchi, R. (1975). Acoustic Emission due to deformation twinning in titanium and Ti – 6Al – 4V alloy. *Scripta Met.,*Vol.9, No.7, pp.777-780.

Vinogradov, A. (1998). Acoustic emission in ultra-fine grained copper. *Scripta Mateialia,* Vol.39, No.6, (August 1998), pp.797-805, 1359-6462.

Valiev, R.Z.; Ismagaliev, R.K & Alexandrov, I.V. (2000). Bulk nanostructured materials from severe plastic deformation. *Progress in Materials Science*, Vol.45, No.2, pp.103-189, ISSN 0079-6425.

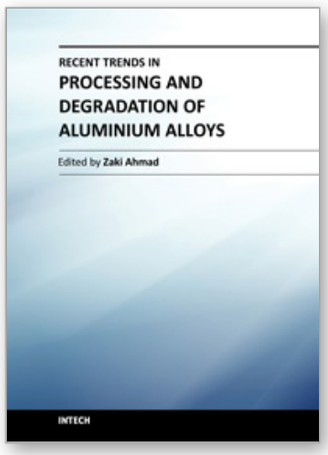

Recent Trends in Processing and Degradation of Aluminium Alloys
Edited by Prof. Zaki Ahmad

ISBN 978-953-307-734-5
Hard cover, 516 pages
Publisher InTech
Published online 21, November, 2011
Published in print edition November, 2011

In the recent decade a quantum leap has been made in production of aluminum alloys and new techniques of casting, forming, welding and surface modification have been evolved to improve the structural integrity of aluminum alloys. This book covers the essential need for the industrial and academic communities for update information. It would also be useful for entrepreneurs technocrats and all those interested in the production and the application of aluminum alloys and strategic structures. It would also help the instructors at senior and graduate level to support their text.

How to reference
In order to correctly reference this scholarly work, feel free to copy and paste the following:

Andrzej Pawelek (2011). Mechanical Behavior and Plastic Instabilities of Compressed Al Metals and Alloys Investigated with Intensive Strain and Acoustic Emission Methods, Recent Trends in Processing and Degradation of Aluminium Alloys, Prof. Zaki Ahmad (Ed.), ISBN: 978-953-307-734-5, InTech, Available from: http://www.intechopen.com/books/recent-trends-in-processing-and-degradation-of-aluminium-alloys/mechanical-behavior-and-plastic-instabilities-of-compressed-al-metals-and-alloys-investigated-with-i

INTECH
open science | open minds

InTech Europe
University Campus STeP Ri
Slavka Krautzeka 83/A
51000 Rijeka, Croatia
Phone: +385 (51) 770 447
Fax: +385 (51) 686 166
www.intechopen.com

InTech China
Unit 405, Office Block, Hotel Equatorial Shanghai
No.65, Yan An Road (West), Shanghai, 200040, China
中国上海市延安西路65号上海国际贵都大饭店办公楼405单元
Phone: +86-21-62489820
Fax: +86-21-62489821

IntechOpen